Paper:
Matthews, J., Owen, G., McEwen, L., Shakesby, R., Hill, J., Vater, A. & Ratcliffe, A. (2017). Snow-avalanche impact craters in southern Norway: Their morphology and dynamics compared with small terrestrial meteorite craters. *Geomorphology, 296*, 11-30.
http://dx.doi.org/10.1016/j.geomorph.2017.08.041

Snow-avalanche impact craters in southern Norway: their morphology and dynamics compared with small terrestrial meteorite craters.

John A. Matthews[1*], Geraint Owen[1], Lindsey J. McEwen[2], Richard A. Shakesby[1], Jennifer L. Hill[2], Amber E. Vater[1] and Anna C. Ratcliffe[1]

[1] *Department of Geography, College of Science, Swansea University, Singleton Park, Swansea SA2 8PP, Wales, UK*

[2] *Department of Geography and Environmental Management, University of the West of England, Frenchay Campus, Coldharbour Lane, Bristol BS16 1QY, UK*

* Corresponding author: J.A.Matthews@Swansea.ac.uk

ABSTRACT

This regional inventory and study of a globally uncommon landform type reveals similarities in form and process between craters produced by snow-avalanche and meteorite impacts. Fifty-two snow-avalanche impact craters (mean diameter 85 m, range 10–185 m) were investigated through field research, aerial photographic interpretation and analysis of topographic maps. The craters are sited on valley bottoms or lake margins at the foot of steep avalanche paths (α = 28–59°), generally with an easterly aspect, where the slope of the final 200 m of the avalanche path (β) typically exceeds ~15°. Crater diameter correlates with the area of the avalanche start zone, which points to snow-avalanche volume as the main control on crater size. Proximal erosional scars ('blast zones') up to 40 m high indicate up-range ejection of material from the crater, assisted by air-launch of the avalanches and impulse waves generated by their impact into water-filled craters. Formation of distal mounds up to 12 m high of variable shape is favoured by more dispersed down-range deposition of ejecta. Key to the development of snow-avalanche impact craters is the repeated occurrence of topographically-focused snow avalanches that impact with a steep angle on unconsolidated sediment. Secondary craters or pits, a few metres in diameter, are attributed to the impact of individual boulders or smaller bodies of snow ejected from the main avalanche. The process of crater formation by low-density, low-velocity, large-volume snow flows occurring as multiple events is broadly comparable with cratering by single-event, high-density, high-velocity, small-volume projectiles such as small meteorites. Simple comparative modelling of snow-avalanche events associated with a crater of average size (diameter 85 m) indicates that the kinetic energy of a single snow-avalanche impact event is two orders of magnitude less than that of a single meteorite-impact event capable of producing a crater of similar size, which is consistent with the incremental development of snow-avalanche impact craters through the Holocene.

Key words:
Snow avalanche impact craters, crater formation, impact processes, meteorite craters, kinetic energy, southern Norway

1. Introduction

Snow-avalanche impact can produce a range of spectacular erosional and depositional landforms (Luckman et al., 1994). These have been described as erosional depressions, impact pits, scour pits, pools, plunge-pools and craters, with associated depositional tongues, mounds, ridges, spreads and ramparts. Such features are relatively well known in Norway (Liestøl, 1974; Corner, 1980; Hole, 1981, Blikra et al., 1989; Blikra and Nemec, 1998; Matthews and McCarroll, 1994; Owen et al., 2006; Matthews et al., 2015) and examples have also been recognised in other avalanche-prone regions, including the North American Cordillera (Davis, 1962; Smith et al, 1994; Johnson and Smith, 2010), the Southern Alps of New Zealand (Fitzharris and Owens, 1984), the Highlands of Scotland (Ballantyne, 1989), and the English Lake District (Brown et al., 2011; Evans et al., 2015; Hambrey and Alean, 2017).

Corner (1980) first recognised three types of snow-avalanche impact landforms: (1) tongue-shaped debris accumulations on the banks of rivers or streams (avalanche-impact tongues); (2) more-or-less circular water-filled depressions in valley bottoms with an associated tongue of debris (avalanche-impact pits); and (3) submerged depressions near lake shorelines surrounded by submerged or partly submerged arcuate ridges of debris (avalanche-impact pools). These features are formed close to the foot of steep mountain slopes by the excavation, ejection and subsequent deposition of unconsolidated sediment following snow-avalanche impact on the river channel, the valley floor or the lake floor, respectively.

Many of the erosional landforms produced by snow-avalanche impact, particularly those of Corner's (1980) second type, resemble small craters produced by volcanic and anthropogenic explosions and meteorite impact (see, for example, Moore, 1976; Roddy et al., 1977; Melosh, 1996, 2011). Indeed, snow-avalanche and meteorite craters provide, at least at first sight, an example of equifinality – i.e. apparently similar landforms produced by different geomorphological processes (Haines-Young and Petch, 1993; Beven, 1996; Beven and Freer, 2001).

Corner (1973, 1975) originally believed a crater-like pit in northern Norway (Rundvatnet) to be a meteorite impact crater but, amongst other evidence, the observation by Liestøl (1974) of a snow avalanche contributing debris to a snow-avalanche impact tongue convinced him otherwise. Unlike craters produced by other possible crater-forming processes, however, those produced by snow-avalanche impact generally result from a relatively long history of frequent avalanching (multiple events) in the same location, rather than from a single large impact event (cf. Owen et al., 2006; Matthews et al., 2015). Snow-avalanche impact craters also exhibit other differences from meteorite craters, which are highlighted in this paper. Nevertheless, the morphology of snow-avalanche impact craters and their similarity to small meteorite impact craters point to the high-energy nature of their formative processes.

Previous research into snow-avalanche impact landforms has focused on particular cases or a small number of examples. In this paper, a much larger number (52) of snow-avalanche impact pits and pools with crater-like form of various sizes

are investigated from southern Norway, with the aims of generalising and developing better understanding of these enigmatic landforms. Our four-fold objectives are:

- To define the general characteristics and morphological variations exhibited by snow-avalanche impact craters;
- To relate crater morphology to landscape setting and the topography of snow-avalanche paths;
- To infer the specific geodynamic processes involved in the formation of snow-avalanche impact craters, such as snow flow, air launch, erosion, debris ejection and deposition; and
- To explore further the similarities and differences between snow-avalanche and meteorite impact craters, including their comparative energies.

2. Study area

Snow-avalanche impact craters were investigated in a broad region of alpine mountain landscape extending across Møre og Romsdal into Sogn og Fjordane Fylke (county) of southern Norway (Figure 1). Many of those found in Møre og Romsdal are associated with 'boulder mounds formed by avalanches' depicted on a map of the Quaternary geology and geomorphology of the Romsdalsalpane-Valldalen area (Carlson et al., 1983). Craters shown on this map were investigated in Meiadalen, Valldalen, Djupdalen and Muldalen, and around Taskedalsvatnet, Brekkevatnet and Yste Brynbotnvatnet. Other craters from Møre og Romsdal were studied in Norangsdalen, Strandadalen, Haugedalen, Frøysadalen/Vatnedalen, and Fedalen. From Sogn og Fjordane, craters were investigated in Glomsdalen and Skjærdingsdalen. These cases represent almost all avalanche-impact landforms with crater-like morphology within the region. Numerous additional river-bank forms (Corner's type 1), some of which have been previously investigated (e.g. Matthews and McCarroll, 1994; Matthews et al., 2015), were excluded from this study on the grounds that the presence of a substantial river channel prevents the development of the full crater form (see discussion below).

The craters have been excavated in unconsolidated till, glaciofluvial deposits, colluvium or lacustrine sediments on valley floors and in lake beds close to shorelines (see specific site descriptions in Section 4). The sediments themselves are derived from the migmatitic and granitic gneissic rocks that predominate in this region of southern Norway (Sigmond et al., 1984; Tveten et al., 1998; Solli and Nordgulen, 2008). Most of the impacted sediments have accumulated since regional deglaciation, which occurred at these sites either following rapid wastage of the Late Weichselian Ice Sheet after ~15,000 calendar years BP (Goehring et al, 2008; Stroeven et al., 2016), or following similar rapid retreat of the Younger Dryas Ice Sheet at the transition to the Holocene after ~11,700 calendar years BP (Nesje, 2009; Mangerud et al., 2011), depending on location. It is likely, therefore, that crater formation has taken place throughout the region over at least the last 10,000 years (see also Matthews and Wilson, 2015).

Snow depths in the region under current conditions are some of the greatest in southern Norway (http://www.senorge.no/). Mean annual snowfall amount is at least 2–4m with >4m characteristic of the snow-avalanche start zones on the upper valley-

side slopes. Snow-avalanche events occur most frequently in spring and early summer with peak activity in March, April and May when large, wet snow avalanches, initiated as slab avalanches and involving the full depth of the snowpack, are characteristic (Laute and Beylich, 2014a).

3. Methodology

The study is based on field observation, aerial photograph interpretation and morphometric analysis of topographic maps. Craters were visited in the field over several years and aerial photographs taken between 1965 and 2013 were downloaded from the *Norge i bilder* website (http://www.norgeibilder.no/). Corresponding topographic maps were obtained from the *Atlas norge* website (http://atlas.no/) on which the latest aerial photographs are also available and can be superimposed on topographic maps.

Parameters used in this paper to analyse crater morphology in relation to topography of the avalanche path are defined in Figure 2 and as follows, based partly on established practice in relation to snow-avalanche and meteorite craters (cf. Laute and Beylich, 2014a; Lied and Toppe, 1989; Lied et al., 1989; McClung and Lied, 1987; McClung and Schaerer, 2006; Melosh, 1996; Osinski and Pierazzo, 2013).

D = crater diameter = diameter of the crater rim determined from erosional scars; the minimum (d_{min}) distance across the crater rim is used for non-circular craters;

W = crater-wall height = maximum height of the crater rim above water level in the crater (or crater floor where the crater is dry), determined from the height of proximal (w_p) or distal (w_d) erosional scars (whichever is the greater) or apparent mound height (m) in the absence of any erosional scar;

A = start zone area = potential area of the avalanche path within which avalanches are initiated (the avalanche source area);

aspect = aspect of the avalanche path (start zone and track) according to eight sectors of the compass;

H = vertical drop of the entire length of the avalanche path = vertical distance from the highest point of the starting zone (the starting point) to the crater (the stopping point);

L = avalanche path length = horizontal distance from the starting point to the crater centre;

h = vertical drop of the final 200 m length (ℓ_{200}) of the avalanche path;

α = mean slope angle of the entire avalanche path from the starting point to the centre of the crater;

β = mean slope angle of the lower avalanche path defined as the final 200 m length (ℓ_{200}) of the avalanche path;

Crater diameters, normally represented by water-filled depressions in the land surface, were measured from aerial photographs to an estimated accuracy of ±5 m. The height of erosional scars (representing crater walls) and depositional mounds (representing the sedimentary material ejected from the crater) were estimated to ±2 m during field visits to the sites. These parameters underestimate the crater-wall

height of water-filled craters but were used because water depth in the craters is unknown in all but a few cases. Start zones and avalanche paths were defined from contours on the maps combined with the geomorphological evidence of erosional tracks, surviving deposits of avalanche snow, and vegetation differences, all detectable on aerial photographs and/or observed in the field. As well as the obvious destruction of trees in avalanche tracks below the tree line, other vegetational indicators include contrasting plant communities reflecting environmental gradients of disturbance and snow tolerance (Butler, 1979; Malanson and Butler, 1984; Erschbaumer, 1989; Walsh et al., 2004, 2009; Bebi et al., 2009). The area of each avalanche start zone was estimated to ±1000 m^2 from maps enlarged to a scale of 1:14,000. The same maps, with a contour interval of 20 m, were used to construct long-profiles (thalwegs) of each avalanche path. Further heights and angles were measured on the long profiles with an estimated accuracy of ±5 m and ±1°, respectively.

Standard statistical techniques of parametric and non-parametric correlation were used to analyse interrelationships between crater size and topographic parameters as a basis for inferring snow-avalanche dynamics. Both types of correlation coefficient were used to ensure that interpretations based on parametric coefficients were not unduly affected by data characteristics.

A simple modelling exercise was used to estimate the kinetic energy (KE) of snow-avalanche and meteorite events capable of producing a small crater with the average diameter of our snow-avalanche examples (85 m). KE values for single impact events were derived by combining both our and published data in the fundamental equation, $KE = 0.5mv^2$, where m = mass and v = velocity on impact. Calculation of the mass of snow in a crater-forming avalanche was based on the average avalanche source area (A), shown in Table 1 (approximately 10,000 m^3), with snow depth based on the minimum snowfall (1 m) associated with major avalanches (Armstrong and Williams, 1992; Pudasaini and Hutter, 2007). A value of 100 kg/m^3 was used for the density of freshly fallen snow based on values of 50-200 kg/m^3 given in the literature (Judson and Doesken, 2000). Estimates of the velocity of moving avalanches range widely. During snow-avalanche descent, a core (~1–5 m deep) of relatively high-density (~100–300 kg/m^3), fast-flowing snow (~20–60 m/s for dry snow; lower for wet snow) occurs near the base of the flow (McClung and Schaerer, 2006). We use a value of 25 m/s.

The likely characteristics of projectiles associated with meteorite impact craters 85 m in diameter were estimated from the literature on confirmed small meteorite craters (see below). Assuming a spherical meteorite, the available data suggest a mass of the order of 10,000 kg, based on a meteorite diameter of 2 m and densities ranging from 4000 kg/m^3 for stony to 8000 kg/m^3 for iron meteorites (Henderson, 1954; Britt and Consolmagno, 2003), and an impact velocity of the order of ~5,000 m/s (Kofman et al., 2010; Folco et al., 2011).

4. Specific sites and craters

All the investigated craters are located on the maps in Figure 3, which also show the topographic setting of each crater. Further details of selected craters are shown in the aerial photographs of Figure 4 and the terrestrial photographs of Figures 5 and 6.

4.1 Taskedalsvatnet (Craters 1-5)

Five craters were identified at Taskedalsvatnet (Figure 3A). Erosional scars of various sizes characterise the crater walls. Particularly large, semi-circular proximal scars, like those of Craters 3 and 4 (Figure 5A), are termed 'blast zones' in this paper (see also discussion below). Craters 2–5 are typical examples of snow-avalanche impact pools (*sensu* Corner, 1980), the distal crater rims of which are partially submerged arcuate ridges that extend a few metres above lake level on the distal side of the pools (Figure 5A). Crater No.1 can be described as a snow-avalanche impact pit (*sensu* Corner, 1980), though its elongated shape in the direction of the small stream draining through it from Taskedalsvatnet is not typical, and is a feature suggestive of Corner's (1980) snow-avalanche impact tongues.

4.2 Brekkevatnet (Craters 6-11)

Four of the six craters at Brekkevatnet (Figure 3B) are snow-avalanche impact pools, of which Crater 6 is a particularly impressive example with a circular crater, well-developed, arcuate, distal ridge extending out into the lake and a large proximal blast zone (Figures 4A and 5B). Crater 7 is a snow-avalanche impact pit with a major distal ridge (Figures 4B and 5C) and other ridge fragments or mounds beyond this and to either side of the water-filled depression. Its distal scar is well developed but the proximal scar is almost nonexistent (Figure 4B). The separate, much smaller pit (Crater 8), located to the NE of Crater 7, has the typical circular form of a crater, and a separate avalanche path is identifiable, but the distal ridge and both distal and proximal scars are indistinct (Figures 4B and 5D). The three pools on the south side of the lake (Craters 9–11) have well-developed proximal blast zones and submerged distal ridges clearly visible on the aerial photographs dating from 2003. A single boulder associated with the distal ridge at Crater 9 is the only point at which these distal ridges extend above the lake level. The craters at Brekkevatnet illustrate well the existence of widely differing crater morphology within a small area.

4.3 Ytste Brynbotnvatnet (Craters 12-14)

All three snow-avalanche impact pools at Ytste Brynbotnvatnet (Figure 3C) have well-developed proximal blast zones, but only the largest crater (No. 12) has a distal mound, which extends to the north as a submerged ridge. The distal ridges of the smaller craters on the eastern side of the lake (Nos 13 and 14) have distinct arcuate proximal scars but are more difficult to define because they are submerged in relatively deep water.

4.4 Meiadalen (Craters 15-16)

Two of the largest snow-avalanche impact pits included in this study occur in Meiadalen, where they comprise part of Slettvikvatnet and the whole of Øvstevatnet (Craters 15 and 16, respectively; Figure 3D). The latter crater is another particularly spectacular example because of its large size, well-developed proximal blast zone and

broad low distal mound that almost completely encloses Øvstevatnet (Figures 4C and 5E). The maximum depth of this crater-lake (8.2 m) was measured by Matthews et al. (2011).

4.5 Langdalen Farm, Valldalen (Craters 17-18)

These two very small but clear snow-avalanche impact pits with small proximal scars and distal mounds, which are separated by a river terrace riser, occur on the western side of Valldalen near Langdalen Farm (Figures 3E). Although a single avalanche path has been identified in Figure 3E, beginning at 1300 m on Krikefjellet and ending at the two craters, the uniform topography of the valley side may have reduced the accuracy of the lateral limits of the starting zones and avalanche tracks. At least three even smaller pits (termed 'secondary craters' in the discussion below) are located a few metres from the main craters, two of which are shown in Figure 4D.

4.6 Fremste Heivatnet (Craters 19-20)

Two snow-avalanche impact pools with large proximal blast zones are the product of snow-avalanches descending from the eastern slopes of Middagshornet and Trollkyrkja, respectively, on the western side of Fremste Heivatnet (Figure 3F). The rim of the larger crater (No. 20) is well defined on three sides by the blast zone (Figure 5F), whereas that of Crater 19 is less extensive but is defined by a distinct proximal scar and a submerged ridge discernible on aerial photographs. A further well-defined semicircular scar can be recognised in the south-eastern corner of the lake but is not included in our sample of craters because the avalanche path could not be identified.

4.7 Djupdalsvatnet (Craters 21-23)

All three snow-avalanche impact pools in Djupdalsvatnet tend towards an oval shape in plan as defined by their proximal blast zones and distal submerged ridges (Figure 3G).

4.8 Muldalen (Craters 24-26)

The three snow-avalanche impact pits in Muldalen (Figure 3H) represent relatively small circular craters without proximal scars but with well-developed distal mounds. Crater 25 (Figure 5G) is similar to the others. In addition, a much smaller secondary crater (Figure 5H), similar in character to those identified at Langdalen Farm except for a more irregular form, can be seen a few metres to the east of Crater 25.

4.9 Norangsdalen (Craters 27-34)

A total of eight craters have been investigated on the western side of Norangsdalen (Figures 3I and 3J), at the shorelines of a series of four shallow lakes (Gailskredvatnet, Djupvatnet, Urdvatnet and Stavbergvatnet). Most of these well-developed craters can be classified as snow-avalanche impact pools. However, on account of the shallowness of the lakes, the distal mounds tend to extend well above lake level. Many of the proximal scars are well-developed blast zones (Figures 6A-D) and there is also evidence for several other partially formed craters associated

especially with Gailskredvatnet and Djupvatnet (Figure 3I). A detailed case study was carried out of the exceptionally large Crater 33, at the northern end of Urdvatnet (Figures 3J and 6D) by Owen et al. (2006); their bathymetric survey of the plunge pool revealed a remarkable maximum water depth of 11.4 m.

4.10 Røyr Farm, Strandadalen (Crater 35)

The large, oval-shaped snow-avalanche impact pit at Røyr Farm has a well-developed proximal blast zone but only a poorly developed distal mound. A larger mound appears to have been partially levelled for agriculture as a cultivated field extends up to the eastern edge of the crater. The marked oval shape of this crater is clearly related to the presence of a second avalanche track which is aligned towards the lake to the south of the main track (Figure 3K).

4.11 Haugedalsvatnet (Craters 36-38)

The three craters of different sizes at Haugedalsvatnet (Figure 3L) are typical snow-avalanche impact pools with well-developed proximal blast zones and submerged distal ridges.

4.12 Vatnedalsvatnet (Craters 39-47)

The four craters at the southern end of Vatnedalsvatnet (Craters 39–42) are typical snow-avalanche impact pools (Figure 3M) with well-developed proximal blast zones and clear distal ridges that are partly or wholly submerged. The plunge-pools and submerged ridges, with a few boulders extending above lake level, are particularly clear on aerial photographs dating from 2010 (Figure 4E). The five craters nearer the northern end of the lake (Craters 43–47; Figures 3M and 3N) are more varied in character. Crater 45 is a small snow-avalanche impact pool, whereas Craters 43, 44 and 46) are snow-avalanche impact pits. Crater 46 is particularly interesting on account of its almost unbroken circular crater rim, correspondingly complete crater wall and unusually large distal mound. It is also unusual in that the depression behind the mound is not water-filled due to the steepness of the slope of this part of the lower valley-side and the breach at the southern end of the mound. The northernmost Crater 47 is at the south-western extremity of a larger elongated landform that extends towards the northeast on the bank of the river exiting the lake. The elongated form of the ridge can be attributed to the amalgamation of Crater 47 with several small craters in addition to the presence of the river, which suggests the whole landform represents a snow-avalanche impact tongue (*sensu* Corner, 1980).

4.13 Fedalen (Craters 48-49)

Crater 48 is a small, simple, circular snow-avalanche impact pit with proximal scar and distal mound located some distance to the west of the stream flowing northwards through Fedalen (Figures 3O and 4F). This crater is also notable for the dense scatter of boulders surrounding the crater on all sides. Crater 49, in contrast, is a more complex landform appearing to consist of at least three proximal scars, which merge to form a well-developed, elongated distal mound on the eastern bank of the stream close to Fedalssætra. It therefore has some of the characteristics of a snow-avalanche impact tongue.

4.14 Nøkkvatnet (Crater 50)

Located close to Glomnessætra, the single large snow-avalanche impact pit in Glomsdalen has a well-developed proximal blast zone, a well-developed distal mound, and a markedly oval shape (Figures 3P, 4G and 6E).

4.15 Skjærdingsdalen (Craters 51-52)

Two merging snow-avalanche impact pits lie close to but separate from the west bank of the Skjerdingsdøla (Figures 3Q, 4H). Crater 51 has an extremely well-developed distal mound (Figure 6F) but no proximal scar, whereas Crater 52 is smaller and less well formed. Two secondary craters are located in hummocky and bouldery terrain to the north of Crater 52.

5. Results

Profiles of the avalanche paths are shown in Figure 7 and morphometric data relating to the craters and avalanche tracks are summarised in Table 1 and Figure 8.

Crater diameter (D) ranges from 10 to 185 m with a mean of 85 m: 90% of craters have a diameter between 25 and 150 m, and 68% a diameter between 50 and 100 m. Crater wall height (W) ranges from 1 to 40 m with a mean of 13 m (median 10 m). These measures of crater size are associated with an avalanche start zone area (A) of 18,000 to 467,000 m^2 (mean, 108,000 m^2), a mean avalanche path length (L) of 928 m, a vertical drop (H) of at least 200 m (mean, 672 m) and a path slope angle (α) of at least 28° (mean 35.6°, 80% between 30 and 45°). The slope angle of the final 200 m (ℓ_{200}) of the avalanche path (β) is lower than that of the entire path in every case (mean 21.6°; 85% between 15 and 30°). The avalanche paths have a strong preferred easterly aspect, with 60% facing directly E and >90% facing NE, E or SE (Figure 8H).

Pearson's product-moment correlation coefficient ($r = 0.81$; $p<0.001$) and Spearman's non-parametric correlation coefficient ($rho = 0.82$; $p<0.001$) indicate that D and W are strongly and positively correlated. It is notable that this strong relationship between these two crater parameters is highly statistically significant, despite the differing level of skew shown in Figures 8A and 8B. Correlation analysis of these characteristics of crater size and the topographic parameters (Table 2) indicates some other relationships that are relatively weak but nevertheless statistically significant. Using the results of Pearson's correlation coefficient, D is significantly correlated with A ($r = 0.31$; $p<0.05$) but not with the slope of the final 200 m of the avalanche path (β). W, on the other hand, is significantly correlated with β ($r = 0.34$; $p<0.02$) with only a marginally significant correlation with A ($r = 0.25$; $p<0.10$). None of the other measured topographic parameters is significantly related to either D or W, and results based on Spearman's rho are closely similar to those based on Pearson's r.

The results from comparative modelling of the kinetic energy involved in forming a snow-avalanche crater of average size (diameter 85 m) are summarised in

Table 3. It is estimated that the kinetic energy of a typical large snow-avalanche associated with our impact craters is 3.1 x 10^9 J. This contrasts with an estimated kinetic energy of the order of 1.3 x 10^{11} J for the correspondingly sized meteorite impact crater.

6. Discussion

6.1 General characteristics of the craters related to avalanche paths

Avalanche-impact craters examined in this study tend towards a circular shape, with typical diameters of 50-100 m and steep proximal crater walls 5–15 m in height. Distal crater walls tend to be lower, absent or replaced by relatively low depositional mounds. Our craters invariably occur at the foot of steep, east-facing avalanche paths, which are typically ~30° or steeper over their whole length and >15° over the final 200 m, and are characterised by potential avalanche start areas mostly within the range 50,000–150,000 m^2.

The strong correlation between crater diameter (D) and crater wall height (W), with coefficients of determination (r^2) >65%, indicates the latter to be a meaningful parameter relating to crater size, which is here regarded as a surrogate for crater depth (even though W is measured relative to water level in the crater). Furthermore, as crater diameter is more strongly related than crater wall height to avalanche start area (A), it seems to be related to snow-avalanche volume. It should be recognised, however, that the volume of individual snow-avalanche events are likely to be overestimated by A.

Although crater wall height, and hence crater depth, is more closely related to the slope of the lower avalanche track (β), the pattern of correlations involving crater wall height is explained by crater wall height being essentially a measure of proximal scar height (proximal scars are generally much larger than those associated with distal mounds, if present). Proximal scar height in turn reflects the angle of slope into which the scar is eroded. For craters of similar size, steeper slopes result in the larger scars, and the absence of proximal scars is a feature of avalanche paths with a low β angle.

Slope angles (α) of our crater-forming avalanche paths are similar to those of the start zones and tracks of non-crater-forming avalanche paths. Start zones of all types of the latter are usually restricted to angles of 30°–50°, occasionally 60° (Perla, 1977; Schweizer and Jamieson, 2001; Schweizer et al., 2003; Pudasaini and Hutter, 2007). The lowermost part of the avalanche path of non-crater-forming avalanches is generally characterised by a runout zone which, on slopes of 5–10°, can extend for distances of 300–500m (McClung et al., 1989; Perla and Martinelli, 2004). Typical slope angles for such runout zones are 15° or less and, when predicting runout distances, an angle of 10° is commonly used in defining the beginning of the runout zone (McClung and Schaerer, 2006). In contrast, for our crater-forming avalanche paths, β is <10° in only one out of the 52 cases, and <15° in only four cases. Thus, there can be no doubt that (1) the lower path angle (β) of crater-forming avalanches is appreciably steeper than the comparable slope angles associated with non-crater-forming avalanches and (2) absence of a run-out zone appears to be a general characteristic of crater-forming avalanche paths. We conclude, therefore, that typical

craters form where a sufficiently large volume of avalanche snow impacts unconsolidated sediment at the valley floor and/or the lake floor, at a sufficiently steep angle.

The easterly aspect of the vast majority of the avalanche paths clearly results mainly from greater snow accumulation on lee-side locations under the prevailing westerly wind regime in southern Norway. Avalanche activity in southern Norway, as elsewhere, reflects the complex interaction between terrain, snowpack and meteorological conditions (Schweizer et al., 2003; Ancey, 2006; Eckerstorfer and Christiansen, 2011; Laute and Beylich, 2014a). All of our avalanches start in the alpine zone, above the tree line, where the absence of trees favours avalanche initiation (Pudasaini and Hutter, 2007), whereas many of our craters are located in the sub-alpine zone. The presence of trees has little or no effect on crater formation, however, because trees are either swept away or never develop fully in snow-avalanche tracks subject to frequent avalanche events.

More than 80% of all avalanches take place after heavy snowfalls, which is related to snow loading and to the inherent weakness of fresh snow: snowfalls <15 cm rarely produce avalanches, and snowfalls >1 m are able to produce major avalanches (Armstrong and Williams, 1992; Pudasaini and Hutter, 2007). The timing and frequency of snow avalanches for two valleys within the study region have been shown to be controlled mainly by snowfall intensity, intervals with strong winds leading to snow drifting, and/or sharp changes of air temperature, all within the March to May peak avalanche season (Laute and Beylich, 2014a, 2014b). Heavy rainfall can also be an important trigger late in the avalanche season.

Although inter-annual variability in snow-avalanche activity is high (Laute and Beylich, 2014a), the spatial distribution of avalanches is often strongly localised (Luckman, 1977; Stoffel et al., 1998). Snow avalanches are generally more frequent in start zones with concave cross-slope profiles (Gleason, 1995; McClung, 2001) and may be further channelled in the avalanche-track zone. Such topographic focusing is particularly important with respect to the location of craters, where a sufficient volume of snow must be repeatedly transported towards approximately the same point at the foot of the avalanche path. While topographic focusing accounts for the compact, near-circular shape of the craters, avalanche volume appears, in large part, to account for crater size. The elongated shape of a minority of the craters, in which the longest axis is aligned at right angles to the avalanche path, is accounted for by variation in the precise route taken by successive avalanches down the same general path (such as Nos 1, 35 and 50) and/or by the merger of two or more craters (Nos 47 and 49).

6.2 Processes of cratering in relation to avalanche impact dynamics

Understanding of the processes of impact crater formation comes largely from studies of meteorite impact craters (Melosh, 1996; Collins et al., 2012; Osinski and Pierazzo, 2013; Osinski et al., 2013a). Such craters are excavated where the transfer of energy during sudden contact of a ‘projectile’ or ‘impactor’ (the moving material) with a ‘target’ (the impacted material) generates sufficient pressure to initiate a shock wave that penetrates the target and sets the material behind in motion, leading to an upward and outward ‘excavation flow’ and the ejection of target material. As the shock wave

549 propagates into the target, the excavated material is directed radially away from the
550 impact site in an 'impact plume' and deposited as an 'ejecta blanket' leaving a
551 hemispherical crater in all but the most oblique impacts. Crater planform tends
552 towards an ellipse (with long axis in the direction of motion of the projectile) only at
553 impact angles of <10–15°. Thus, as 90% of meteorites impact at 15–70° to the Earth's
554 surface, most meteorite craters are circular (Pierazzo and Melosh, 2000; Davison et
555 al., 2011).
556
557 The main difference between vertical and oblique impacts is the fate of the
558 projectile material which, at high impact angles, is directed radially away from the
559 impact site (Melosh, 1996; Pierazzo and Melosh, 2000). In the case of vertical
560 impacts, ejecta are evenly distributed in all directions. In oblique impacts of 60–45°,
561 the ejecta form downrange and uprange jets with most material being directed
562 downrange, in the direction of motion of the projectile. At impact angles of 45–30°
563 the uprange jet no longer forms, so its ejecta are absent, and as the angle decreases
564 still further to 20–10°, ejecta-free regions appear in both uprange and downrange
565 directions (Osinski et al., 2011). Similar processes appear to be directly applicable to
566 cratering produced by snow-avalanche impact.
567
568 Impact pressure of snow in motion is proportional to the snow density and the
569 square of the velocity (McClung and Schaerer, 1985, 2006). In contrast to the
570 associated much lower density snow cloud (two orders of magnitude less dense than
571 in the core), it is the high-density flow that creates the impact pressures (~1000 kPa)
572 capable of moving reinforced concrete structures (McClung and Schaerer, 2006;
573 Sovilla et al., 2008) and, by implication, excavating craters. Nevertheless, as snow
574 densities are an order of magnitude less than the 1500–2700 kg m^{-3} densities in rock
575 avalanches and other types of landslides (Zitti et al., 2016), impact pressures
576 associated with snow avalanches are proportionately less. Presumably, therefore, the
577 latter do not excavate craters because their velocity is less, the material in motion is
578 more dispersed (i.e. not focused on a small area), or the angle of impact is too low.
579 Perhaps, however, there are crater floors beneath the debris of some rock avalanches.
580
581 Lack of any significant correlation (Table 2) between crater size (*D* or *W*) and
582 either the length (*L*) or slope (α) of the avalanche path, or the vertical drop (*H*), are
583 inferred to indicate the overriding importance of start zone area and snow volume on
584 crater size. However, the correlations between crater size and start zone area appear to
585 be moderated by other topographic factors which have not been quantified. Convex
586 downslope curvature of the avalanche path, and microtopographic unevenness, favour
587 not only avalanche formation by provoking stress concentrations (Schweizer et al.,
588 2003) but also the air launch of avalanches. Air launch results in increased velocity by
589 reducing friction with the ground and increasing the impact angle on landing, both of
590 which promote crater expansion by increasing impact pressure. Such irregularities in
591 the profiles in Figure 7, especially if they are present near the bottom of the avalanche
592 path, suggest that air launch is likely to be important in the formation of many of the
593 craters.
594
595 Because of the prevailing climate in southern Norway, almost all our craters
596 are water-filled and are likely to be ice-covered in spring and early summer when
597 most snow avalanches occur, introducing a second potential moderating factor.
598 Neither water nor ice appears necessary, however, for crater formation. Indeed, Crater

46 is unlikely ever to have contained water owing to its position on a valley side slope. In addition, the water in many craters is extremely shallow. In such cases, the impact pressure produced by snow-avalanching is unlikely to differ substantially from that associated with avalanching onto *terra firma*. Deeper water layers reduce crater size and crater formation will be completely suppressed in very deep water (cf. Dypvik and Jansa, 2003; Wünnemann et al., 2010).

A third potential factor moderating the direct effect of snow-avalanche volume is the effect of waves generated by snow-avalanche impact on a water body. When a snow avalanche enters a substantial body of water, as is the situation for the majority of craters in this study, momentum and energy of the avalanche mass are transferred to the water, creating an initial hydrodynamic crater, the collapse of which produces an impulse wave (tsunami-like wave) with possible seiche effects (produced by oscillatory waves) within the confined space defined by the walls of the impact crater (Fritz, 2002; Fritz et al., 2003; Heller et al., 2009; Zitti et al., 2016). Collapse of the hydrodynamic crater may cause a backward-moving (up-range) impulse wave to entrain an air cavity against the proximal crater wall. The subsequent collapse of the air cavity and the resulting rebound produces an almost vertical jet (Fritz et al., 2003), as produced by underwater explosions (Le Méhauté and Wang, 1996). We propose, therefore, that impulse waves are likely to contribute to the enlargement of our water-filled craters and, in particular, help explain large-scale proximal scars, which are aptly termed 'blast zones'. A forward-moving (down-range) impulse wave, in contrast, is more likely to disperse, be less explosive, and simply overtop low distal mounds accounting, at least in part, for the relatively small size or absence of distal scars.

Craters with large erosional proximal blast zones associated with steep β angles, high impact angles and air-launched avalanches therefore contrast with those characterised by small or absent proximal scars, shallow β angles and relatively low angles of impact. The distal mounds composed of material ejected forwards from the craters tend, where present, to be very variable in their height and shape, reflecting more complex interactions between depositional and erosional processes associated with avalanches of varying frequency and magnitude (cf. Owen et al., 2006). Distal mounds produced in association with snow-avalanche impact craters also differ from the landforms produced by purely depositional types of snow avalanche (cf. Rapp, 1959; Luckman, 1977, 2004; Jomelli and Francou, 2000; Jomelli and Bertran, 2001). The primary process of deposition of snow-avalanche impact mounds is essentially grain-flow dumping from the atmosphere though other processes, such as snow ploughing, may modify existing mound deposits.

Distal mounds almost invariably consist of a single low ridge. Presence of more than one ridge, as at Crater 7 (Figure 4B) and Crater 31 (Figure 6B and 6C), is unusual but may indicate avalanches of differing magnitude, while absence of a distal mound often suggests erosive rather than depositional avalanche activity on the distal side of the crater, as at Crater 33 (Figure 6D; see also Owen et al., 2006). Another unusual feature is the existence of distal scars on both sides of the distal mound at Crater 6 (Figure 4A). The scar on the distal side of the mound appears to indicate that some high-magnitude avalanche events land in Brekkevatnet after travelling over the crater and clearing the distal mound.

The phenomenon of 'secondary craters' (close to Craters 17, 18, 25 and 52) seems largely unrelated to the above discussion. These very small pits are more irregular in shape than the primary craters, generally lack proximal or distal scars, and tend to be elongated with the long axis parallel to the avalanche path. We suggest such secondary craters are the product of individual boulders and/or snow parcels thrown out/ejected during snow-avalanche transport or impact, a conclusion supported by individual large boulders immediately adjacent to some of these pits (Figure 4D) and the distal boulder pile associated with the pit close to Crater 25 (Figure 5H).

6.3 Comparison of snow-avalanche craters with small meteorite craters

The smallest known meteorite impact craters on Earth are of comparable size to the snow-avalanche impact craters investigated in this study. Often, small meteorite craters exist in clusters or crater fields, each crater being produced by the impact of a fragment of a larger meteoroid that disintegrated during its passage through Earth's atmosphere (Passey and Melosh, 1980). The Henbury craters, located in arid central Australia, are typical examples of small meteorite craters (Hodge, 1965; Buhl and McColl, 2015). Thirteen confirmed craters have been recognised at Henbury, ranging from 6 m to 146 m in diameter with crater walls rising up to 4.5 m above the surrounding terrain and up to 16 m above dry crater floors. Other confirmed meteorite craters of similar size to our avalanche-impact craters, most of which were formed in the Holocene and have been well preserved, many under arid climatic regimes, are listed in Table 4.

Similarities in size and form between small meteorite craters, defined here as less than ~200 m in diameter, and our snow-avalanche impact craters of a similar size indicate parallels in the crater formation process. Small meteorite impact craters are produced by small-volume, high-density projectiles (meteorites) travelling at high velocity. Snow-avalanche impact craters, on the other hand, are produced by relatively large-volume, low-density, low-velocity snow flows. The different combinations of projectile size, density and velocity have produced similar cratering effects, suggesting closely related processes and approximate equivalence of impact energy and pressures (see below).

It must be emphasised, however, that we are suggesting equivalence of process and effect between snow-avalanche and meteorite cratering only in relation to small meteorite craters produced by relatively low-energy impacts. 'Simple' (bowl-shaped) meteorite craters include some that are relatively large compared to avalanche examples, the iconic Meteor Crater (Barringer Crater), Arizona, at 1.2 km diameter being a case in point (Hodge, 1994; Melosh and Collins, 2005; Kring, 2007; Newsom et al., 2013). Equivalence between snow-avalanche and meteorite impact craters is more difficult to sustain in relation to such large 'simple' meteorite craters as well as larger 'complex' meteorite craters, both of which are produced by very high velocity (hypervelocity) impacts (French, 1998; Osinski and Pierazzo, 2013).

Even when comparisons are made between craters of similar size, there remain some important differences between craters formed by meteorite and snow-avalanche impact. Such differences should enable the development of diagnostic criteria for separating the two types of craters and also point to the fallacy of the concept of equifinality – i.e. once landforms are examined in detail, those formed by different

processes are, in fact, seen not to be identical. First, snow-avalanche impact craters do not form the perfectly circular bowl-shaped depressions approximated by most well-developed and well-preserved meteorite impact craters of the simple type. This can be attributed in large part to snow-avalanche impact craters resulting from the cumulative effects of many avalanches that vary in their magnitude and in the precise position of the avalanche track (see below). In contrast, meteorite impact craters are clearly single-event phenomena.

Second, where meteorite craters are elliptical rather than circular, their long axes tend to be aligned with the direction of motion and can usually be attributed to oblique impact. Our asymmetrical avalanche-impact craters, on the other hand, invariably have long axes aligned at right angles to the direction of the avalanche track, which is attributable to multiple avalanche events. For these features, successive avalanches do not follow exactly the same path but tend to divert to one side or the other of a central target point.

Third, the rims of most meteorite craters usually form an unbroken ring around the excavated crater, whereas the distal mounds of our snow-avalanche craters typically occupy less than half the circumference of the crater. Snow-avalanche craters where the ejecta are evenly distributed around the entire circumference of the crater (e.g. Crater 48, Figure 4F), are rare and only seem to occur in the case of craters located well away from the valley side. Furthermore, in the case of Crater 48, ejecta are widely dispersed rather than concentrated in a narrow rim. This can be explained by the occurrence of snow-avalanche impact craters close to the foot of steep slopes. Deposition of ejecta in such cases can only occur in the down-range direction: the up-range effect is primarily erosional, producing the erosional proximal scars (blast zones) discussed above.

Fourth, meteorite craters commonly have raised rims formed from the uplift of target material, which commonly includes bedrock, as well as the deposition of ejecta (Kenkmann et al., 2013). None of our craters is excavated in bedrock and the associated distal mounds appear not to be affected by such impact tectonics but to owe their elevation above the surrounding terrain entirely to the deposition of ejecta derived from unconsolidated sediment.

Fifth, the ejecta from snow-avalanche craters appear to be unaffected by any kind of impact metamorphism, which changes rocks and minerals as a result of extreme shock, temperature or pressure associated with hypervelocity impact (Ferrière and Osinski 2013; Osinski et al., 2013b). The impactites produced by meteorite impact range from completely reconstituted lithologies, such as impact-melt rocks, to fractured target rock, such as impact breccia (Stöffler and Grieve, 2007; Grieve and Therriault, 2013). Further research is required, however on the ejecta from snow-avalanche craters, to determine whether the redeposited sediment possesses any diagnostic characteristics other than super-angular edges.

Finally, a distinction needs to be made between various types of primary and secondary impact craters. The secondary craters identified close to Craters 17, 18, 25 and 52 in our study have been attributed to individual boulders and/or snow packets, the impacts of which are minor in comparison to the impact of the main body of flowing snow in the snow avalanche itself. In meteorite crater fields, small craters

produced by ejecta deposited beyond the continuous ejecta blanket that surrounds a primary crater are also termed secondary craters (Melosh, 1996; McEwen et al., 2005). While many of these are due to relatively small projectiles or fragments of projectiles that travel at hypervelocities and therefore produce high-pressure shock waves and other effects typical of primary meteorite impact craters, the smallest (metre-size) of these, which lose most of their kinetic energy in the atmosphere and therefore impact at much lower velocity, have been termed 'impact holes', 'meterorite pits', 'dug craters', 'penetration craters' or 'penetration funnels' (Krinov, 1960, 1963; Elston and Scott, 1971; Hodge, 1994; Wright et al., 2007; Osinski and Pierazzo, 2013). The numerous 'impact holes' associated with the Sikhote-Alin meteorite impact (Table 4) are of this type; they appear closely analogous to our 'secondary craters' but are clearly different from most 'secondary craters' in crater fields associated with primary meteorite craters. These considerations raise the question: how similar are the formative mechanisms of primary snow-avalanche impact craters to simple meteorite 'impact holes'?

6.4 Kinetic energy of cratering in relation to the frequency and magnitude of events

The comparison between the kinetic energy of crater-forming snow avalanches and meteorites (Table 3) can only yield approximate values. This is in part because of the many uncertainties associated with the model inputs, and in part because the physics of impact of a dispersed mass (snow avalanche) are likely to differ from those of a dense body (meteorite). Nevertheless, conclusions can be drawn from the orders of magnitude of the derived kinetic energies. Specifically, using typical values as estimates of avalanche parameters, the kinetic energy associated with a crater-forming avalanche, appears to be roughly two orders of magnitude less than for a meteorite capable of excavating a similar-sized crater in a single event. This result supports the interpretation throughout this study that snow-avalanche impact craters do not form in a single event, but develop incrementally over many events.

Based on meteorological and dendrochronological studies in Bødalen, to the west of the Jostedalsbreen ice cap in southern Norway, extreme-magnitude snow-avalanche events over the last 100 years have a recurrence interval of 15–20 years (Decaulne et al., 2014). Furthermore, an investigation of the lacustrine sediments in neighbouring Oldenvatnet, recognised 47 snow-avalanche event layers deposited during the last 7,300 years (Vasskog et al., 2011). This represents a recurrence interval of ~155 years for the extremely large avalanches capable of reaching the lake and depositing sufficient debris. Combining these two records while ignoring differences in the magnitude of the recorded events and possible decadal- to millennial-scale variability in the frequency of avalanches (cf. Blikra and Selvik, 1998; Nesje et al., 2007; Vasskog et al., 2011) suggests a recurrence interval for major snow-avalanche events within a range of ~15–150 years. If this is assumed to be applicable to snow-avalanche impact craters throughout the region since regional deglaciation, i.e. for at least the last ~10,000 years (see above), it can be inferred that at least ~60 and possibly >600 avalanches contributed to the excavation of each crater. These numbers are consistent with the conclusion from our modelling that the kinetic energy of a single crater-forming snow-avalanche event is two orders of magnitude less than that of the equivalent meteorite-impact event associated with a crater of the same size.

7. Conclusion

(i). This study has investigated a large sample of 52 snow-avalanche impact craters from southern Norway, adding substantially to understanding the general nature and variations exhibited by this little-known but spectacular landform, and pointing out similarities to small craters produced by meteorite impact.

(ii). Most snow-avalanche impact craters are approximately circular. They range in diameter from 10 to 185 m (mean diameter 85 m in this study) and fall into one of two categories of snow avalanche-impact landforms, termed snow-avalanche impact pits and snow-avalanche impact pools by Corner (1980). The former are located in valley-bottom sites; the latter are sited close to the shoreline of lakes in shallow water. Almost all are water-filled with rims defined by proximal erosional scars (blast zones) up to 40 m high and much lower (<12 m high) distal erosional scars and/or distal depositional mounds, which are largely submerged in the case of the snow-avalanche impact pools.

(iii). All snow-avalanche impact craters are located close to the foot of steep (α = 28–59°) valley-side slopes where the gradient of the final 200 m of the avalanche path (β) typically exceeds ~15°. Crater diameter (D) is significantly but weakly correlated ($r = 0.312$; $p<0.05$) with the potential avalanche start zone area (A), which varies from 18,000–467,000 m^2, but not with the vertical drop (H) or length (L) of the avalanche path, or α. A strong correlation ($r = 0.81$; $p<0.001$) between D and crater wall height (W) demonstrates that both are measures of crater size and a weaker correlation (0.342; $p<0.02$) between W and β suggests proximal scars are largest when they are eroded into relatively steep valley sides. In contrast, crater size is more closely related to avalanche volume than to the major topographic characteristics of the avalanche path.

(iv) The key requirements for the development of snow-avalanche impact craters (pools and pits), as opposed to purely depositional types of snow-avalanche landforms, are the repeated occurrence of topographically-focused, large-volume and high-velocity snow avalanches that impact with a steep angle on unconsolidated sediment on the valley or lake floor.

(v). Proximal blast zones indicate up-range ejection of avalanche material (sediment, water and ice) from the craters and are associated with the steep impact angles of the snow avalanches. Formation of such erosional scars is assisted by air-launch of avalanches (caused by topographical irregularities in the profile of the avalanche path) and by impulse waves generated by high-angle impact into water-filled craters. Formation of generally low distal mounds with, in some cases, distal scars, indicates more dispersed down-range deposition of ejecta and both erosional and depositional controls.

(vi). Secondary snow-avalanche impact craters or pits, a few metres in diameter and more irregular in shape than primary snow-avalanche impact craters, are attributed to the impact of individual boulders and/or relatively small parcels of snow ejected from the main avalanche.

(vii). There are fundamental similarities in form and process between snow-avalanche impact craters and small (<200 m diameter) meteorite impact craters. Cratering in single events by high-density, high-velocity, small-volume meteorite projectiles is therefore broadly equivalent to cratering in repeated events by relatively low-density, low-velocity, large-volume snow flows.

(viii). Simple comparative modelling of snow-avalanches associated with craters of average size (diameter 85 m in this study) indicates that the kinetic energy of a single snow-avalanche impact event is about 3.0×10^9 J, which is two orders of magnitude less than a single meteorite-impact event that produces a crater of the same size. This result is consistent with previously published recurrence intervals of 15–150 years for major avalanches in the study area and the incremental development of the landforms over at least the last 10,000 years of the Holocene.

(ix). Further differences between meteorite impact craters and snow-avalanche impact craters include: departures from circularity exhibited by some snow-avalanche craters; irregularities in snow-avalanche crater rims caused by patterns of erosion and deposition; the effects of uplift (impact tectonics) in elevating the rims of meteorite impact craters; the excavation of avalanche craters only in unconsolidated sediment (whereas meteorite craters are commonly excavated in bedrock); impact metamorphism, which apparently only affects meteorite craters; and differences in the causes of 'secondary craters'. All of these differences raise important questions for further research. They also demonstrate that considering snow-avalanche and meteorite craters as an example of equifinality is more apparent than real.

Acknowledgements

Fieldwork was carried out on the Swansea University Jotunheimen Research Expeditions, mainly in 2010 and 2011. We are grateful to Roger Matthews for field assistance and to Anders Gjerde for support in Valldalen. This paper constitutes Jotunheimen Research Expeditions, Contribution No. 203 (see http://jotunheimenresearch.wixsite.com/home).

References

Ancey, C. 2006. *Dynamique des Avalanches*. Press Polytechniques Universitaires Romandes, Lausanne.

Armstrong, B.R., Williams, K. 1992. *The Avalanche Book*. Fulcrum Publishing, Golden, CO.

Ballantyne, C.K. 1989. Avalanche impact landforms on Ben Nevis, Scotland. *Scottish Geographical Magazine* 105, 38–42.

Bebi, P., Kulakowski, D., Rixen, C. 2009. Snow avalanche disturbances in forest ecosystems — State of research and implications for management. *Forest Ecology and Management* 257: 1883–1892.

Bevan, A., McNamara, K. 1993. *Australia's Meteorite Craters*. Western Australia Museum, Perth.

Beven, K.J. 1996. Equifinality and uncertainty in geomorphological modelling. In: Rhodes, B.L., Thorn, C.E. (Eds) *The Scientific Nature of Geomorphology.*Wiley, Chichester, pp. 289–313.

Beven, K.J., Freer, J. 2001. Equifinality, data assimilation, and uncertainty estimation in mechanistic modelling of complex environmental systems. *Journal of Hydrology* 249, 11–29.

Blikra, L.H., Nemec, W. 1998. Postglacial colluvium in western Norway: depositional processes, facies and palaeoclimatic record. *Sedimentology* 45, 909–959.

Blikra, L.H., Selvik, S.F. 1998. Climatic signals recorded in snow avalanche-dominated colluvium in western Norway: depositional facies successions and pollen records. *The Holocene* 8, 631–658.

Blikra, L.H., Hole, P.A., Rye, N. 1989. Skred i Norge. Hurtige massebevegelser og avsetningstyper i alpine områder, Indre Nordfjord. *Norges Geologiske Undersøkelse, Skrifter* 92, 1–17.

Britt, D.T., Consolmagno, S.J. 2003. Stony meteorite porosities and densities: a review of the data through 2001. *Meteoritics and Planetary Science* 38, 1161–1180.

Brown, V.H., Evans, D.J.A., Evans, I.S. 2011. The glacial geomorphology and surficial geology of the south-west English Lake District. *Journal of Maps* 2011, 221–243.

Buhl, S., McColl, D. 2015. *Henbury Craters and Meteorites: Their Discovery, History and Study, 2nd edition*. Springer International Publishing, Switzerland.

Butler, D.R. 1979. Snow avalanche path terrain and vegetation, Glacier National Park, Montana. *Arctic and Alpine Research* 11, 17–32.

Carlson, A.B., Sollid, J.L., Torp, B. 1983. *Valldal Kvartaergeologi og Geomorphologi, 1319 IV [Valldal Quaternary Geology and Geomorphology, Sheet 1319 IV] 1: 50,000.* Oslo, Geografisk Institutt, Universitetet i Oslo.

Cassidy, W.A., Renard, M.L. 1996. Discovery research value in the Campo del Cielo. Argentina, meteorite craters. *Meteoritics and Planetary Science* 31, 433–448.

Classen, J. 1978. The meteorite craters of Morasko in Poland. *Meteoritics* 13(2), 245–255.

Collins, G.S., Melosh, H.J., Osinski, G.R. 2012. The impact-cratering process. *Elements* 8, 25–30.

Corner, G.D. 1973. Meteorittkrater i Tromsø? *Ottar* 76, 13–14.

Corner, G.D. 1975. Rundvatnet — avalanche plunge-pool or meteorite impact crater? *Norsk Geografisk Tidsskrift* 29, 75-76.

Corner, G.D. 1980. Avalanche impact landforms in Troms, North Norway. *Geografiska Annaler, Series A (Physical Geography)* 62, 1–4.

Davis, G.H. 1962. Erosional features of snow avalanches, Middle Fork Kings River, California. *United States Geological Survey Professional Paper* 450D, 122–125.

Davison, T.M., Collins, G.S., Elbeshausen, D., Wünnemann, K., Kearsley, A.T. 2011. Numerical modelling of oblique hypervelocity impacts in strong ductile targets. *Meteoritics and Planetary Science* 46, 1510–1524.

Decaulne, A., Eggertsson, Ó., Laute, K., Beylich, A.A. 2014. A 100-year extreme snow-avalanche record based on tree-ring research in upper Bødalen, inner Nordfjord, western Norway. *Geomorphology* 218, 3–15.

Dypvik, H., Jansa, L.F. 2003. Sedimentary signatures and processes during marine bolide impacts: a review. *Sedimentary Geology* 161, 309–337.

Eckerstorfer, M., Christiansen, H.H. 2011. Topographical and meteorological control on snow avalanching in the Longyearbyen area, central Svalbard 2006-2009. *Geomorphology* 134, 186–196.

Elston, D.P., Scott, G.R. 1971. Pueblito de Allende penetration craters and experimental craters formed by free fall. *Journal of Geophysical Research* 76, 5756–5764.

Erschbaumer, B 1989. Vegetation on avalanche paths in the Alps. *Vegetatio* 80, 139–146.

Evans, D.J.A., Brown, V.H., Roberts, D.H., Innes, J.B., Bickerdike, H.L., Vieli, A., Wilson, P. 2015. Wasdale Head. In: McDougall, D.A., Evans, D.J.A. (Eds) *The Quaternary of the Lake District: Field Guide.* Quaternary Research Association, London, pp. 213–238.

Ferrière, L., Osinski, G.R. 2013. Shock metamorphism. In: Osinski, G.R., Pierazzo, E. (Eds) *Impact Cratering: Processes and Products*. Wiley-Blackwell, Chichester, pp. 106–124.

Fitzharris, B.B., Owens, I.F. 1984. Avalanche tarns. *Journal of Glaciology* 30, 308–312.

Folco, L., Di Martino, M., El Barkooky, A., D'Orazio, M., Lethy, A,. Urbini, S., Nicolosi, I., Hafez, M., Cordier, C., van Ginneken, M., Zeoli, A., Radwan, A.M., El Khrepy, S., El Gabry, M., Gomaa, M., Barakat, A.A., Serra, R., El Sharkawi, M. 2011. Kamil Crater (Egypt): ground truth for small-scale meteorite impacts on Earth. *Geology* 39, 179–182.

French, B.M. 1998. *Traces of Catastrophe: A Handbook of Shock-Metamorphic Effects in Terrestrial Meteorite Impact Structures. LPI Contribution No. 954*. Lunar and Planetary Institute, Houston, TX.

Fritz, H.M. 2002. *Initial phase of landslide generated impulse waves*. Doctor of Technical Sciences Thesis, ETH Zürich, Zürich.

Fritz, H.M., Hager, W.H., Minor, H.-E. 2003. Landslide generated impulse waves. 2. Hydrodynamic impact craters. *Experiments in Fluids* 35, 520–532.

Gleason, J.A. 1995. Terrain parameters of avalanche starting zones and their effect on avalanche frequency. *Proceedings of the International Snow Science Workshop, Snowbird, Utah, USA, 30 October-3 November 1994*, 393–404.

Glikson, A.Y., Hickman, A.H., Vickers, J. 2008. Hickman Crater, Ophthalmia Range, Western Australia: evidence supporting a meteorite impact origin. *Australian Journal of Earth Sciences* 55, 1107–1117.

Goehring, B.M., Brook, E.J., Linge, H., Raisbeck, G.M., Yiou, F. 2008. Beryllium-10 exposure ages of erratic boulders in southern Norway and implications for the history of the Fennoscandian Ice Sheet. *Quaternary Science Reviews* 27, 320–336.

Grieve, R.A.F., Therriault, A.M. 2013. Impactitites: their characteristics and spatial distribution. In: Osinski, G.R., Pierazzo, E. (Eds) *Impact Cratering: Processes and Products*. Wiley-Blackwell, Chichester, pp. 43–59.

Gurov, E.P., Gurova, E.P. 1998. The group of Macha craters in western Yakutia. *Planetary and Space Science* 46, 323–328.

Haines, P.W. 2005. Impact cratering and distal ejecta. The Australian record. *Australian Journal of Earth Science* 52, 481–507.

Haines-Young, R.H., Petch, J.R. 1983. Multiple working hypotheses: equifinality and the study of landforms. *Transactions of the Institute of British Geographers* 8, 458–466.

Hambrey, M.J., Alean, J.C. 2017. *Colour Atlas of Glacial Phenomena.* CRC Press, Boca Raton, FL.

Heller, V., Hager, W.H., Minor, H.-E. 2009. *Landslide generated impulse waves in reservoirs: basics and computation.* Versuchsanstalt für Wasserbau, Hydrologie und Glaziologie, ETH Zürich, Zürich.

Henderson, E.P. 1954) A discussion of the densities of iron meteorites. *Geochemica et Cosmochimica Acta* 6, 221–240.

Herd, C.D.K., Froese, D.G., Walton, E.L., Kofman, R.S., Herd, E.P.K., Duke, M.J.M. 2008. Anatomy of a young impact event in central Alberta, Canada: prospects for the missing Holocene impact record. *Geology* 36, 955–958.

Hodge, P.W. 1965. The Henbury meteorite craters. *Smithsonian Contributions to Astrophysics* 8, 199–213.

1048 Hodge, P.W. 1994. *Meteorite Craters and Impact Structures of the Earth*. Cambridge,
1049 Cambridge University Press.
1050
1051 Hole, J. 1981. Groper danna av snøskred i Sunnylven og tilgrensande områder på
1052 Sunnmøre. Førbels resultat. *Norsk Geografisk Tidsskrift* 35, 167–172.
1053
1054 Holliday, V.T., Kring, D.A., Mayer, J.H., Goble, R.J. 2005. Age and effects of the
1055 Odessa meteorite impact, western Texas, USA. *Geology* 33, 945–948.
1056
1057 Johnson, A.L., Smith, D.J. 2010. Geomorphology of snow avalanche impact
1058 landforms in the southern Canadian Cordillera. *The Canadian Geographer* 54, 87–
1059 103.
1060
1061 Jomelli, V., Bertran, P. 2001. Wet snow avalanche deposits in the French Alps:
1062 structure and sedimentology. *Geografiska Annaler, Series A (Physical Geography)*
1063 83, 15–28.
1064
1065 Jomelli, V., Francou, B. 2000. Comparing the characteristics of rockfall talus and
1066 snow-avalanche landforms in an alpine environment using a new methodological
1067 approach: Massif des Ecrins, French Alps. *Geomorphology* 35,181–192.
1068
1069 Judson, A., Doesken, N. 2000. Density of freshly fallen snow in the central Rocky
1070 Mountains. *Bulletin of the American Meteorological Society* 81, 1577–1587.
1071
1072 Kenkmann, T., Artemieva, N.A., Wünnemann, K., Poelchau, M.H., Elbeshausen, D.,
1073 Núñez del Prado, H. 2009. The Carancas meteorite impact crater, Peru: geologic
1074 surveying and modelling of crater formation and atmospheric passage. *Meteoritics*
1075 *and Planetary Science* 44, 985–1000.
1076
1077 Kenkmann, T., Collins, G.S., Wünnemann, K. 2013. The modification stage of crater
1078 formation. In: Osinski, G.R., Pierazzo, E. (Eds) *Impact Cratering: Processes and*
1079 *Products*. Wiley-Blackwell, Chichester, pp. 60–75.
1080
1081 Khryanina, L.P. 1981. Sobolevskiy meteorite crater (Sikhote-Alin' Range)
1082 *International Geology Review* 23, 1–10.
1083
1084 Kofman, R.S., Herd, C.D.K., Froese, D.G. 2010. The Whitecourt meteorite impact
1085 crater, Alberta, Canada. *Meteoritics and Planetary Science* 45, 1429–1445.
1086
1087 Kring, D.A. 2007. *Guidebook to the Geology of Barringer Meteorite Crater, Arizona*
1088 *(aka Meteor Crater). LPI Contribution No. 1355.* Lunar and Planetary Institute,
1089 Houston, TX.
1090
1091 Krinov, E.L. 1960. *Principles of Meteoritics*. Pergamon Press, London.
1092
1093 Krinov, E.L. 1963. The Tunguska and Sikhote-Alin meteorites. In: Middlehurst, B.,
1094 Kuiper, G. (Eds) *The Solar System, Vol.4, Moon, Meteorites and Craters*. University
1095 of Chicago Press, Chicago, pp. 208–234,
1096

Kuźmiński, H. 1980. The actual state of research into the Morasko meteorite and the region of its fall. *Bulletin of the Astronomical Institute of Czechoslovakia* 31, 58–62.

Laute, K., Beylich, A.A. 2014a. Morphometric and meteorological controls on recent snow avalanche distribution and activity on hillslopes in steep mountain valleys in western Norway. *Geomorphology* 218, 16–34.

Laute, K., Beylich, A.A. 2014b. Environmental controls and geomorphic importance of a high-magnitude/low frequency snow avalanche event in Bødalen, Nordfjord, western Norway. *Geografiska Annaler, Series A (Physical Geography)* 96, 465–484.

Le Méhauté, B., Wang, S. 1996. *Water waves generated by underwater explosions*. Technical Report DNA-TR-94-128. Defense Nuclear Agency, Alexandria, VA.

Lied, K., Toppe, R. 1989. Calculation of maximum snow-avalanche run-out distance by use of digital terrain models. *Annals of Glaciology* 13, 164–169.

Lied, K., Sandersen, F., Toppe. R. 1989. Snow-avalanche maps for use by the Norwegian army. *Annals of Glaciology* 13, 170–174.

Liestøl, O. 1974. Avalanche plunge-pool effect. *Norsk Polarinstitutt Arbok* 1972, 179–181.

Luckman, B.H. 1977. The geomorphic activity of snow avalanches. *Geografiska Annaler, Series A (Physical Geography)* 59, 31–48.

Luckman, B.H. 2004. Avalanche, snow. In: Goudie, A.S. (Ed.) *Encyclopedia of Geomorphology, volume 1*. London, Routledge, pp. 41–44.

Luckman, B.H., Matthews, J.A., Smith, D.J., McCarroll, D., McCarthy, D.P. 1994. Snow-avalanche impact landforms: a brief discussion of terminology. *Arctic and Alpine Research* 26, 128–129.

Malanson, G.P., Butler, D.R. 1984. Transverse pattern of vegetation on avalanche paths in the northern Rocky Mountains, Montana. *Great Basin Naturalist* 44, 453–458.

Mangerud, J., Gyllencreutz, R., Lohne, Ø., Svendsen, J.I. 2011. Glacial history of Norway. In: Ehlers, J., Gibbard, P.L., Hughes, P.D. (Eds) *Quaternary Glaciations – Extent and Chronology: a Closer Look*. Amsterdam, Elsevier, pp. 279–298.

Matthews, J.A., McCarroll, D. 1994. Snow-avalanche impact landforms in Breheimen, southern Norway: origin, age and paleoclimatic implications. *Arctic and Alpine Research* 26, 103–115.

Matthews, J.A., Wilson, P. 2015. Improved Schmidt-hammer exposure ages for active and relict pronival ramparts in southern Norway, and their palaeoenvironmental implications. *Geomorphology* 246, 7–21.

Matthews, J.A., McEwen, L.J., Owen, G. 2015. Schmidt-hammer exposure-age dating (SHD) of snow-avalanche impact ramparts in southern Norway: approaches, results and implications for landform age, dynamics and development. *Earth Surface Processes and Landforms* 40, 1705-1718.

Matthews, J.A., Shakesby, R.A., Owen, G., Vater, A.E. 2011. Pronival rampart formation in relation to snow-avalanche activity and Schmidt-hammer exposure-age dating (SHD): three case studies from southern Norway. *Geomorphology* 130, 280–288.

McClung, D.M. 2001. Characteristics of terrain, snow supply and forest cover for avalanche initiation by logging. *Annals of Glaciology* 32, 223–229.

McClung, D.M. Lied, K. 1987. Statistical and geometrical definition of snow avalanche runout. *Cold Regions Science and Technology* 13, 107–119.

McClung, D.M., Schaerer, P. 1985. Characteristics of flowing snow and avalanche impact pressures. *Annals of Glaciology* 6, 9–14.

McClung, D.M., Schaerer, P. 2006. *The Avalanche Handbook*. The Mountaineers Books, Seattle, WA.

McClung, D.M., Mears, A.I., Schaerer, P. 1989. Extreme avalanche run-out: data from four mountain ranges. *Journal of Glaciology* 13, 180–184.

McEwen, A.S., Preblich, B.S., Turtle, E.P., Artemieva, N.A., Golombek, M.P., Hurst, M., Kirk, R.L., Burr, D.M., Christensen, P.R. 2005. The rayed crater Zunil and interpretations of small impact craters on Mars. *Icarus* 176, 351–381.

Melosh, H.J. 1996. *Impact Cratering: a Geological Process*. Oxford University Press, Oxford.

Melosh, H.J. 2011. *Planetary Surface Processes*. Cambridge University Press, Cambridge.

Melosh, H.J., Collins, G.S. 2005. Meteor crater formed by low-velocity impact. *Nature* 434, 157.

Milton, D.J. 1968. The Boxhole meteorite crater. *United States Geological Survey Professional Paper 599-C*. United States Government Printing Office, Washington DC, pp. 1–23.

Moore, H.J. 1976. Missile impact craters (White Sands Missile Range, New Mexico) and implications to lunar research. Contributions to astrogeology. *United States Geological Survey Professional Paper 812-B*. United States Government Printing Office, Washington DC, pp. 1–47.

Nesje, A. 2009. Latest Pleistocene and Holocene alpine glacier fluctuations in Scandinavia. *Quaternary Science Reviews* 28, 2119–2136.

1196 Nesje, A., Bakke, J., Dahl, S.O., Lie, Ø., Bøe, A.G. 2007. A continuous, high-
1197 resolution 8500-yr snow-avalanche record from western Norway. *The Holocene* 17,
1198 269–277.
1199
1200 Newsom, H.E., Wright, S.P., Misra, S., Hagerty, J. 2013. Comparison of simple
1201 impact craters: a case study of meteor and lunar craters. In: Osinski, G.R., Pierazzo, E.
1202 (Eds) *Impact Cratering: Processes and Products*. Wiley-Blackwell, Chichester, pp.
1203 271–289.
1204
1205 Nininger, H.H., Figgins, J.D. 1933. The excavation of a meteorite crater near
1206 Haviland, Kiowa County, Kansas. *Proceedings of the Colorado Museum of Natural*
1207 *History* 12, 9–15.
1208
1209 Nininger, H.H., Huss, G. 1960. The unique meteorite crater at Dalgaranga, Western
1210 Australia. *Mineralogical Magazine* 32, 619–639.
1211
1212 Ormö, J., Koeberl, C., Rossi, A.P., Komatsu, G. 2006. Geological and geochemical
1213 data from the proposed Sirente crater field: new age dating and evidence for heating
1214 of target. *Meteoritics and Planetary Science* 41, 1331–1345.
1215
1216 Osinski, G.R., Pierazzo, E. 2013. Impact cratering: processes and products. In:
1217 Osinski, G.R., Pierazzo, E. (Eds) *Impact Cratering: Processes and Products*. Wiley-
1218 Blackwell, Chichester, pp. 1–20.
1219
1220 Osinski, G.R., Grieve, R.A.F., Tornabene, L.L. 2013a. Excavation and impact ejecta
1221 emplacement. In: Osinski, G.R., Pierazzo, E. (Eds) *Impact Cratering: Processes and*
1222 *Products*. Wiley-Blackwell, Chichester, pp. 43–59.
1223
1224 Osinski, G.R., Grieve, R.A.F., Marion, C., Chanou, A. 2013b. Impact melting. In:
1225 Osinski, G.R.. Pierazzo, E. (Eds) *Impact Cratering: Processes and Products*. Wiley-
1226 Blackwell, Chichester, pp. 125–145.
1227
1228 Osinski, G.R., Tornabene, L.L., Grieve, R.A.F. 2011. Impact ejecta emplacement on
1229 terrestrial planets. *Earth and Planetary Science Letters* 310, 167-181.
1230
1231 Owen, G., Matthews, J.A., Shakesby, R.A., He, X. 2006. Snow-avalanche impact
1232 landforms, deposits and effects at Urdvatnet, southern Norway: implications for
1233 avalanche style and process. *Geografiska Annaler, Series A (Physical Geography)* 88,
1234 295–307.
1235
1236 Passey, Q.R., Melosh, H.J. 1980. Effects of atmospheric breakup on crater field
1237 formation. *Icarus* 42, 211–233.
1238
1239 Perla, R. 1977. Slab avalanche measurements. *Canadian Geotechnical Journal* 14,
1240 206–213.
1241
1242 Perla, R.I., Martinelli Jr, M. 2004. *Avalanche Handbook*. Honolulu, Hawaii,
1243 University Press of the Pacific.
1244

Petaev, M.I. 1991. The Sterlitamak meteorite: A new crater forming fall. *Solar System Research (Astronomicheskii Vestnik)* 26, 82-99 [in Russian].

Pierazzo, E. Melosh, H.J. 2000. Understanding oblique impacts from experiments, observations and modelling. *Annual Review of Earth and Planetary Sciences* 28, 141-167.

Plado, J. 2012. Meteorite impact craters and possibly impact-related structures in Estonia. *Meteoritics and Planetary Science* 47, 1590–1605.

Prescott, J.R., Robertson, G.B., Shoemaker, C., Shoemaker, E.M., Wynn, J. 2004. Luminescence dating of the Wabar meteorite craters, Saudi Arabia. *Journal of Geophysical Research, Planets* 109, E01008.

Pudasaini, S.P., Hutter, K. 2007. *Avalanche Dynamics: Dynamics of Rapid Flows of Dense Granular Avalanches*. Springer Verlag, Berlin.

Rapp, A. 1959. Avalanche boulder tongues in Lappland: a description of little-known landforms of periglacial debris accumulation. *Geografiska Annaler* 41, 34–48.

Raukas, A., Stankowski, W. 2011. On the age of the Kaali craters, Island of Saaremaa, Estonia. *Baltica* 24(1), 37–44.

Raukas, A., Tiirmaa, R., Kaup, E., Kimmel, K. 2001. The age of the Ilumetsa meteorite craters in southeast Estonia. *Meteorics and Planetary Science* 36, 1507–1514.

Roddy, D.J., Pepin, R.O., Merrill, R.B. (Eds) 1977. *Impact and Explosion Cratering*. Oxford, Pergamon. [Proceedings of the Symposium on Planetary Cratering Mechanics, Flagstaff, Arizona, September 13–17, 1976.]

Schweizer, J., Jamieson, J.B. 2001. Snow cover properties for skier triggering of avalanches. *Cold Regions Science and Technology* 33, 207–221.

Schweizer, J., Jamieson, J.B., Schneebeli, M. 2003. Snow avalanche formation. *Reviews of Geophysics* 41, 4/1016/2003.

Sigmond, E.M.O., Gustavson, M., Roberts, D. 1984. *Berggrunnskart over Norge, Målestokk 1:1 million.* Norges geologiske undersøkelse, Oslo.

Smith, D.J., McCarthy, D.P., Luckman, B.H. 1994. Snow-avalanche impact pools in the Canadian Rocky Mountains. *Arctic and Alpine Research* 16, 116–127.

Solli, A., Nordgulen, Ø. 2008. *Bedrock map of Norway and the Caledonides in Sweden and Finland, Scale 1:2 million.* Geological Survey of Norway, Oslo.

Sovilla, B., Schaer, M., Kern, K., Bartelt, P. 2008. Impact pressures and flow regimes in dense snow avalanches observed at the Vallée de la Sonne test site. *Journal of Geophysical Research: Earth Surface* 113, F01010/2008.

Stoffel, A., Meister, R., Schweizer, J. 1998. Spatial characteristics of avalanche activity in an Alpine valley – a GIS approach. *Annals of Glaciology* 26, 329–336.

Stöffler, D., Grieve, R.A.F. 2007. Impactites. In: Fettes, D., Desmons, J. (Eds) *Metamorphic Rocks: a Classification and Glossary of Terms Recommendations of the International Union of Geological Sciences*. Cambridge University Press, Cambridge, pp. 82–92.

Stroeven, A.P., Hättestrand, C., Kleman, J., Heyman, J., Fabel, D., Fredin, O., Goodfellow, B.W., Harbor, J.M., Jansen, J.D., Olsen, L., Caffee, M.W., Fink, D., Lundqvist, J., Rosqvist, G.C., Strömberg, B., Jansson, K.N. 2016. Deglaciation of Fennoscandia. *Quaternary Science Reviews* 147, 91–121.

Tancredi, G., Ishitsuka, J., Schultz, P.H., Harris, R.S., Brown, P., Revelle, D.O., Antier, K., Le Pichon, A., Rosales, D., Vidal, E., Varela, M.E., Sánchez, L., Benavente, S., Bojorquez, J., Cabezas, D., Dalmau, A. 2009. A meteorite crater on Earth formed on September 15, 2007: the Carancas hypervelocity impact. *Meteoritics and Planetary Science* 44, 1967–1984.

Tiirmaa, R. 1992. Kaali craters of Estonia and their meteoritic material. *Meteoritics* 27, 297.

Tveten, E., Lutro, O., Thorsnes, T. 1998. *Geologisk kart over Noreg, bergrunnskart Årdal M 1:125,000.* Norges Geologiske Undersøkelse, Trondheim.

Vasskog, K., Nesje, A., Støren, E.N., Waldmann, N., Chapron, E., Ariztegui, D. 2011. A Holocene record of snow-avalanche and flood activity reconstructed from a lacustrine sedimentary sequence at Oldevatnet, western Norway. *The Holocene* 21, 597–614.

Walsh, S.J., Weiss, D.J., Butler, D.R., Malanson, G.P. 2004. An assessment of snow avalanche paths and forest dynamics using Ikonos satellite data. *Geocarto International* 19 (2).

Walsh, S.J., Butler, D.R., Allen, T.R., Malanson, G.P. 2009. Influence of snow patterns and snow avalanches on the alpine treeline ecotone. *Journal of Vegetation Science* 5, 657–672.

Wright, S.P., Vesconi, M.A., Spagnuolo, M.G., Cerutti, C., Jacob, R.W., Cassidy, W.A. 2007. Explosion craters and penetration funnels in the Campo del Cielo, Argentina crater field. *38th Lunar and Planetary Science Conference, Abstracts #2017*.

Wünnemann, K., Collins, G.S., Weiss, R. 2010. Impact of a cosmic body into Earth's ocean and the generation of large tsunami waves: insight from numerical modelling. *Reviews of Geophysics* 48, RG4006/2010.

Zitti, G., Ancey, C., Postacchini, M., Brocchini, M. 2016. Impulse waves generated by snow avalanches: momentum and energy transfer to a water body. *Journal of Geophysical Research: Earth Surface* 121, 2399–2423.

FIGURE CAPTIONS

Fig. 1. The study region within southern Norway. Boxes identify the areas covered by Figures 3A-Q.

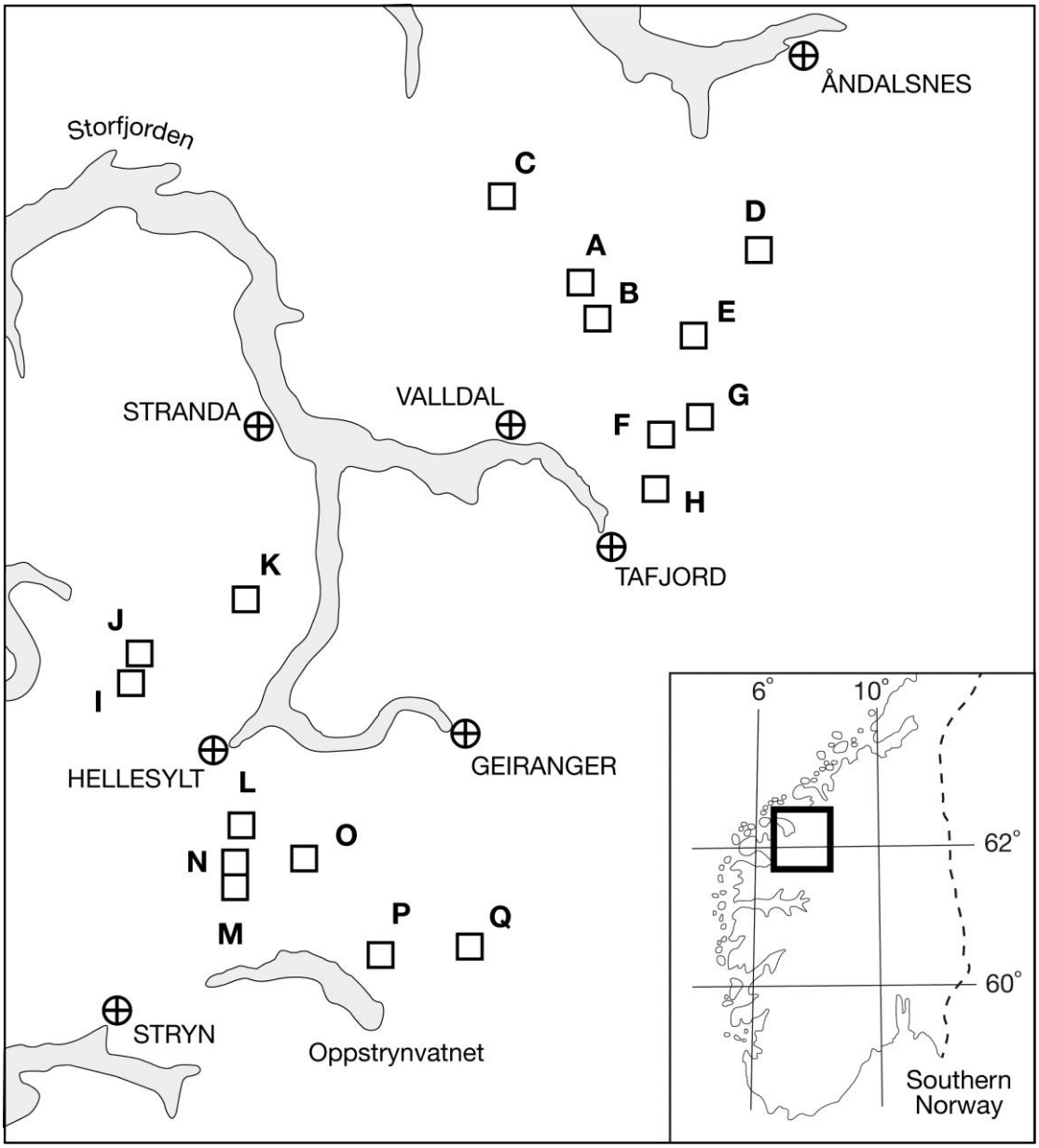

Fig. 2. Terminology of (A) snow-avalanche impact craters and (B) snow-avalanche paths used in this study. Morphological and topographic parameters are defined on plans and profiles of a typical snow-avalanche impact pit and its associated snow-avalanche path. The shaded area is the start zone area (*A*).

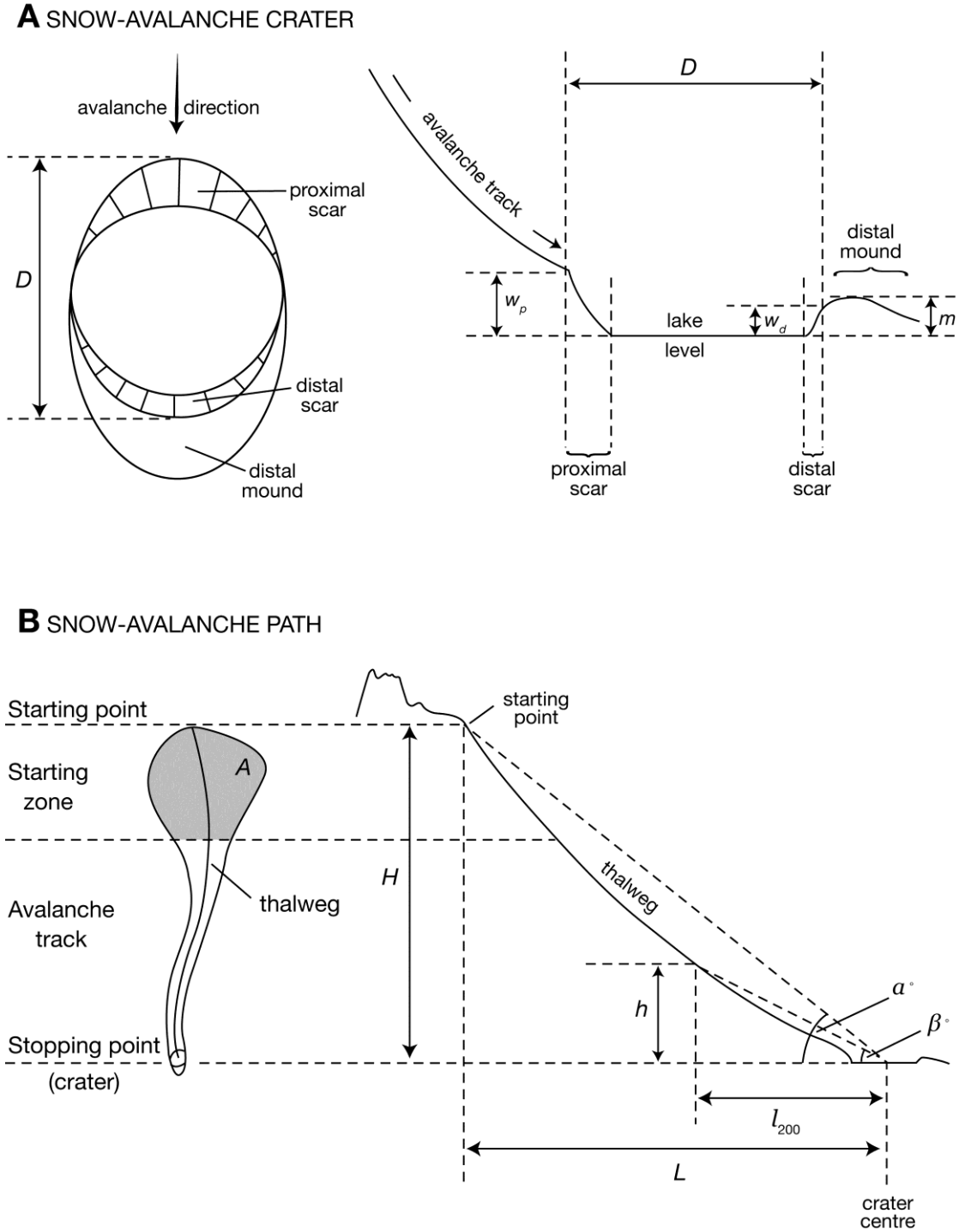

Fig. 3. Maps showing the main features and topographic setting of each snow-avalanche impact crater (numbered) within the specific areas investigated: (A) Taskedalsvatnet; (B) Brekkevatnet; (C) Ytste Brynbotnvatnet; (D) Meiadalen; (E) Langdalen Farm, upper Valldalen; (F) Fremste Heivatnet; (G) Djupdalsvatnet; (H) Muldalen; (I) Norangsdalen (south); (J) Norangsdalen (north); (K) Røyr Farm, Strandadalen; (L) Haugedalsvatnet; (M) Vatnedalsvatnet (south); (N) Vatnedalsvatnet (north); (O) Fedalen; (P) Nøkkvatnet; (Q) Skjærdingsdalen.

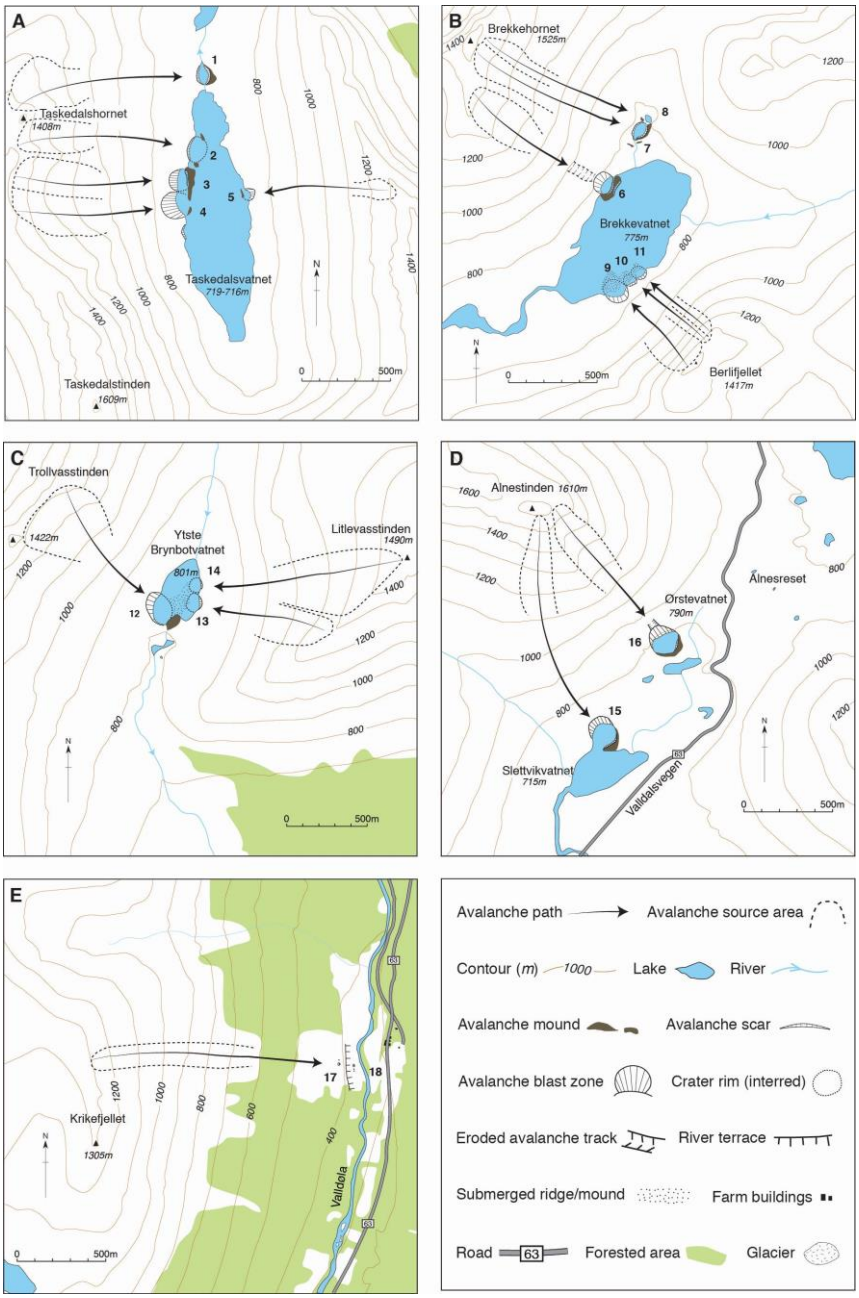

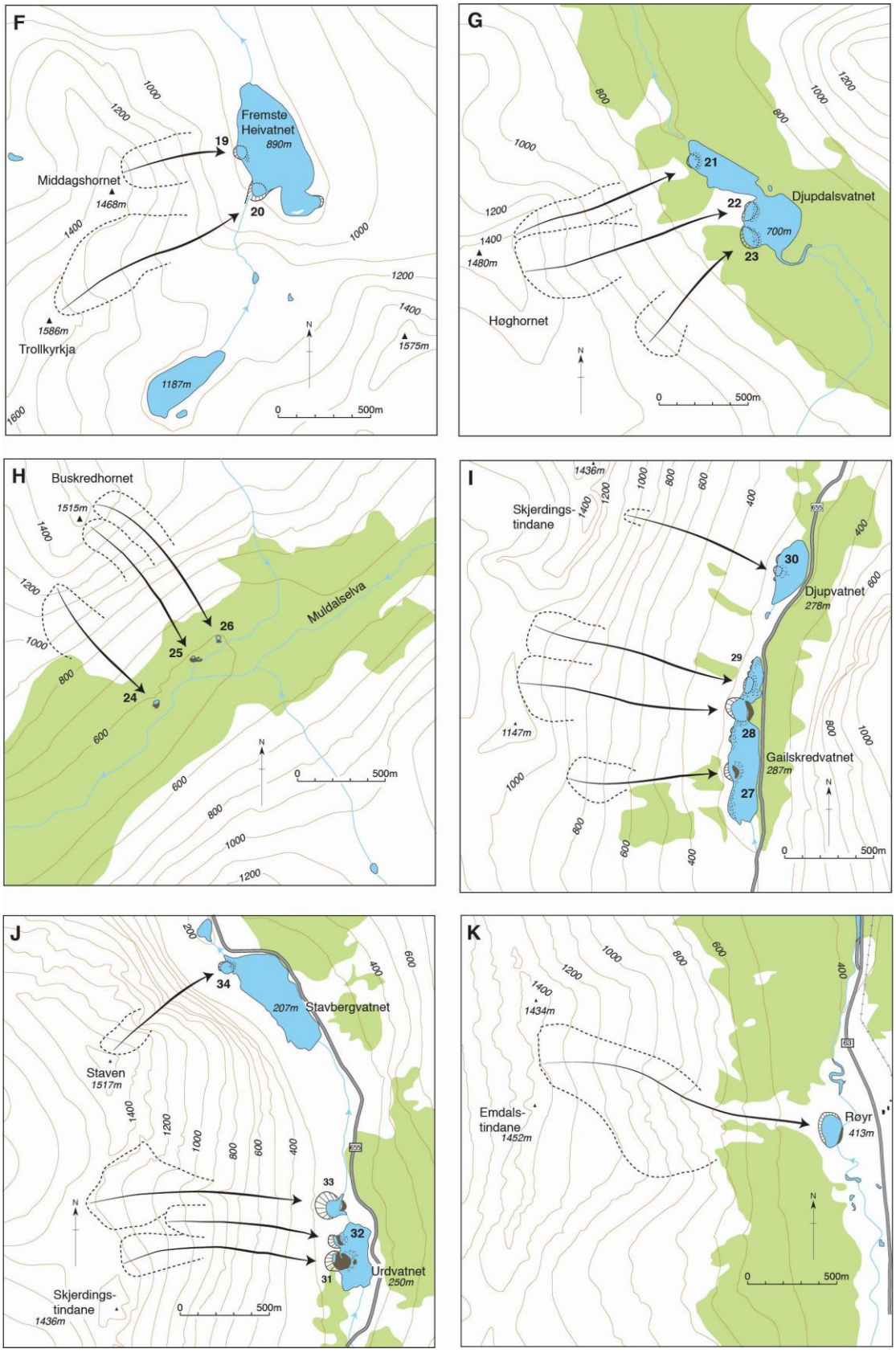
F
Fremste Heivatnet
890m
19
20
Middagshornet
1468m
1586m
Trollkyrkja
1187m
1575m
0
500m
G
21
22
23
Djupdalsvatnet
700m
1480m
Høghornet
H
Buskredhornet
1515m
Muldalselva
24
25
26
I
1436m
Skjerdings-tindane
30
Djupvatnet
278m
29
28
27
Gailskredvatnet
287m
1147m
J
34
207m
Stavbergvatnet
Staven
1517m
33
32
31
Urdvatnet
250m
Skjerdings-tindane
1436m
K
1434m
Emdals-tindane
1452m
Røyr
413m

1367

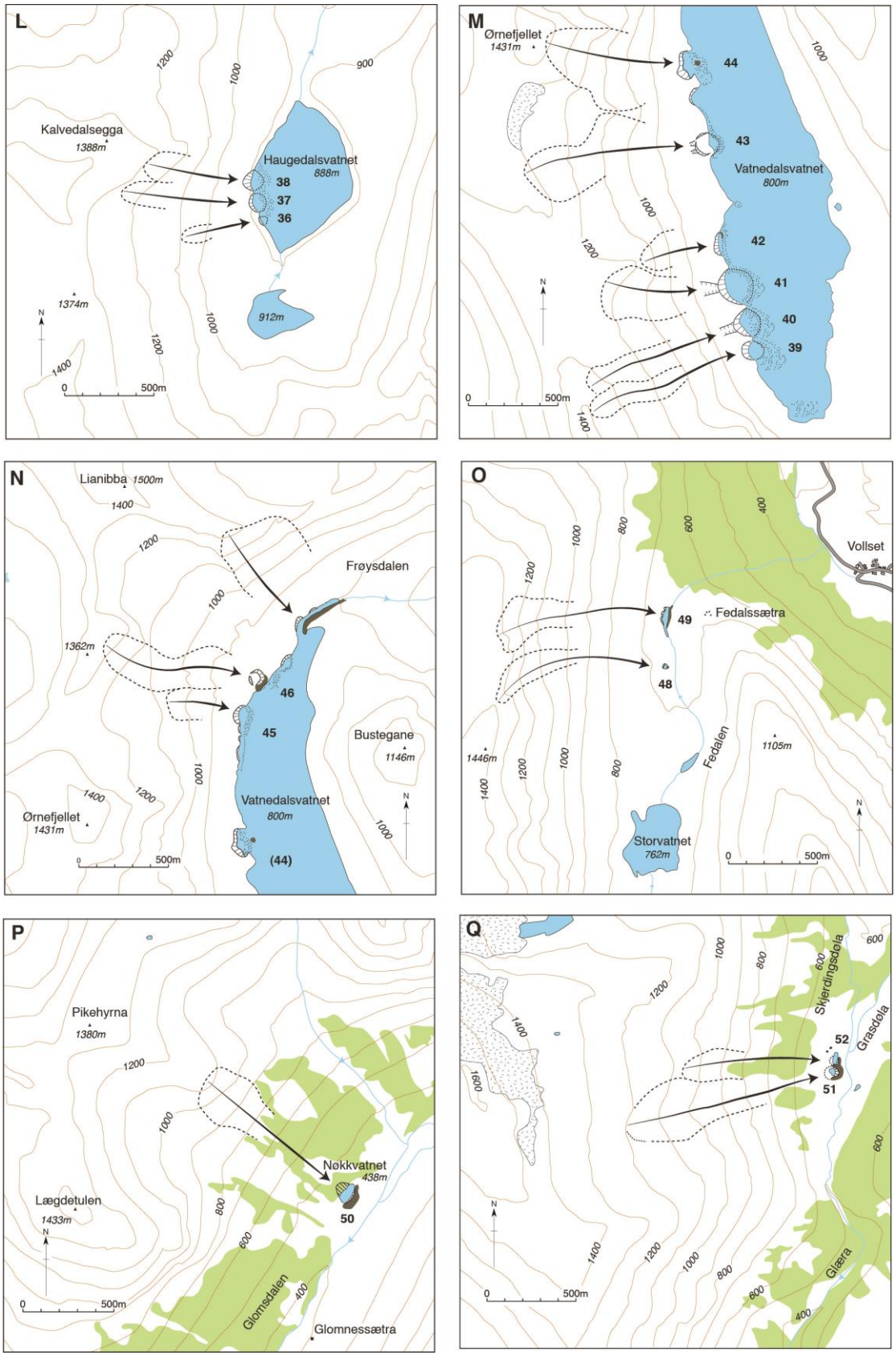
L
Kalvedalsegga
1388m
Haugedalsvatnet
888m
38
37
36
1374m
912m
1200
1000
900
1400
0
500m
M
Ørnefjellet
1431m
44
43
Vatnedalsvatnet
800m
42
41
40
39
1000
1200
1400
N
0
500m
N
Lianibba
1500m
1400
1200
1000
Frøysdalen
1362m
46
45
Bustegane
1146m
Ørnefjellet
1431m
Vatnedalsvatnet
800m
(44)
1400
1200
1000
1000
0
500m
O
Vollset
1200
1000
800
600
400
49
Fedalssætra
48
Fedalen
1105m
1446m
1400
1200
1000
800
Storvatnet
762m
0
500m
P
Pikehyrna
1380m
1200
1000
Nøkkvatnet
438m
50
Lægdetulen
1433m
800
600
400
Glomsdalen
Glomnessætra
0
500m
Q
1000
800
600
1200
1400
1600
Skjerdingsdøla
Grasdøla
52
51
600
1400
1200
1000
800
600
400
Glæra
0
500m

1368

Fig. 4. Aerial photographs of selected craters: (A) Crater 6 in 2013 (Brekkevatnet), a snow-avalanche impact pool with a spectacular proximal erosional scar ('blast zone') and prominent distal ridge; note also the eroded avalanche track and the erosional scars on both sides of the distal ridge; (B) Craters 7 and 8 in 2013 (Brekkevatnet), two snow-avalanche impact pits, both lacking clear proximal erosional scars; (C) Crater 16 in 2014 (Meiadalen), a very large snow-avalanche impact pit with large proximal scar and complete but low distal mound; (D) Crater 18 in 2013 (Langdalen Farm), a small snow-avalanche impact pit with adjacent very small 'secondary craters' possibly caused by the impact of single boulders; (E) Craters 39–40 in 2010 (Vatnedalsvatnet), typical snow-avalanche impact pools exhibiting sub-lacustrine ridges (visible because of relatively shallow water with occasional boulders above lake level separated from the lake shore by pools of deeper water); (F) Crater 48 in 2015 (Fedalen), a small boulder-strewn snow-avalanche impact pit; note especially the even distribution of boulders around this crater; (G) Crater 50 in 2010 (Nøkkvatnet), a large, oval snow-avalanche impact pit with a prominent distal mound and high proximal and distal erosional scars; (H) Crater 51 in 2012 (Skjærdingsdalen), a crater of moderate size with a very well developed distal mound; part of a second, smaller crater is also shown to the north. (Source: http://www.norgeibilder.no/)

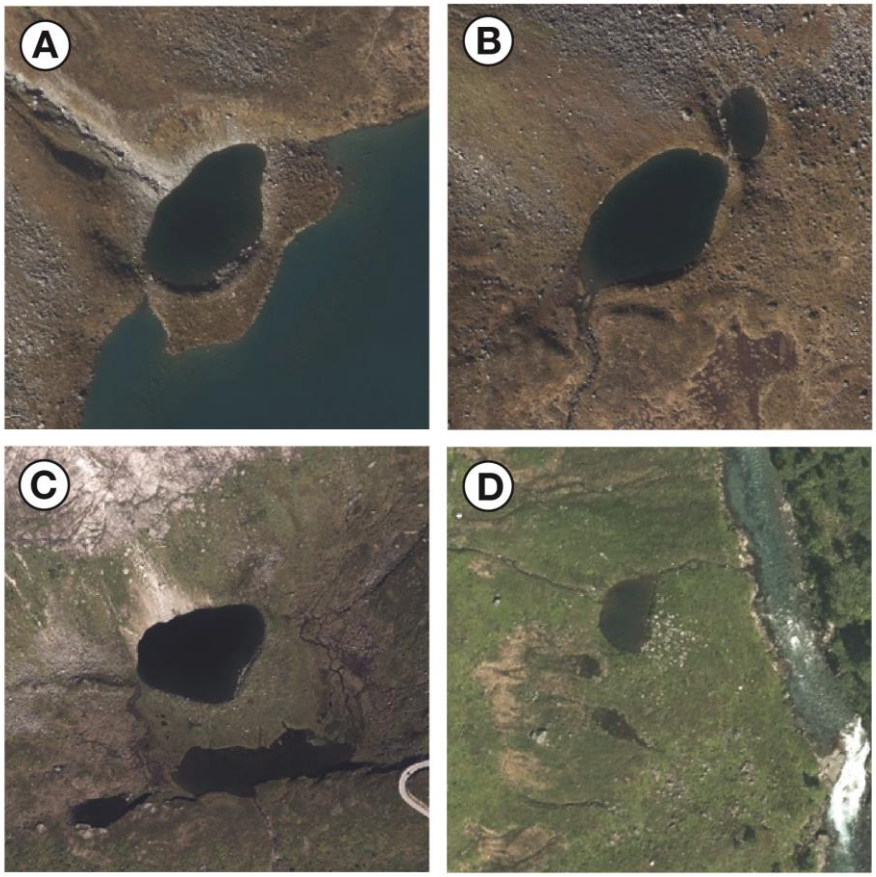

1387

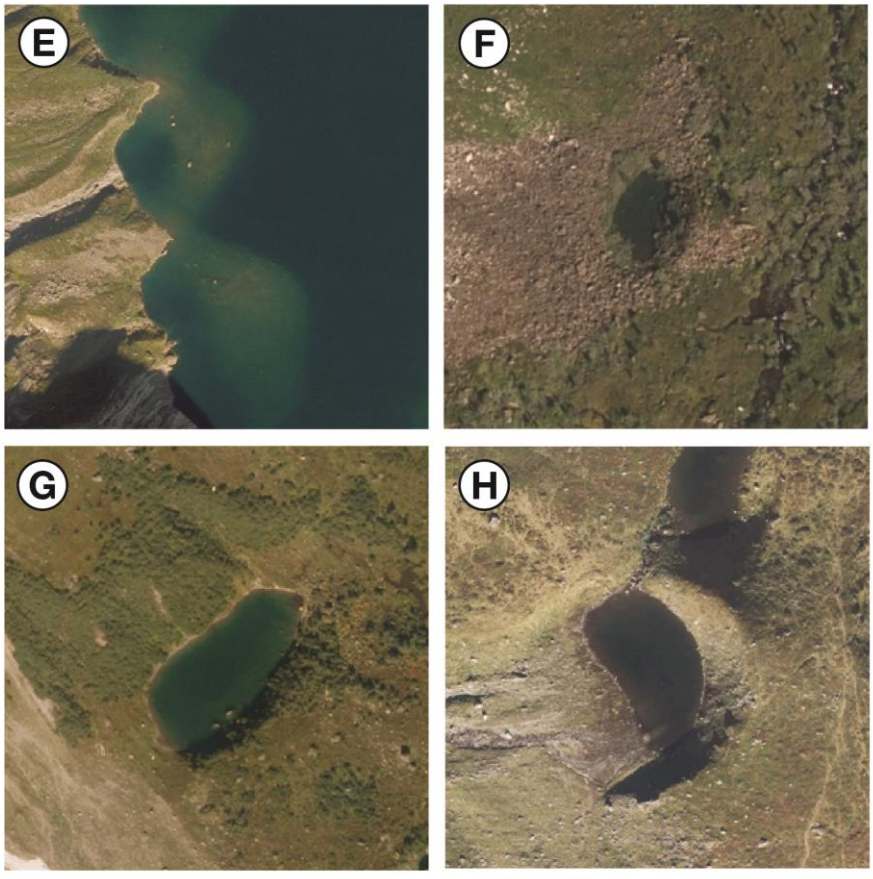

1388

Fig. 5. Terrestrial photographs of selected craters: (A) Craters 3 and 4 (Taskedalsvatnet) in July 2010, with extensive proximal erosional scars ('blast zones') and merged distal mounds forming an off-shore ridge; (B) Crater 6 (Brekkevatnet) in July 2010, showing the large distal mound (height 30 m) littered with debris and snow surviving in the pool from the previous winter (note people for scale); (C) Crater 7 (Brekkevatnet) in July 2010, showing a steep distal scar forming the crater rim on the facing slope of the distal mound; (D) Crater 8 (Brekkevatnet) in July 2010, a small crater (diameter 35 m) viewed from the crest of the distal mound of Crater 7 (note the boulder-strewn slope without a proximal scar; the person on the right stands at the foot of the distal mound of this crater); (E) Crater 16 (Meiadalen) in August 2007, a very large circular crater (diameter 170 m) and proximal scar (height 30 m) with a low but complete distal mound encircling Øvstevatnet and surviving avalanche snow; (F) Crater 20 (Fremste Heivatnet) in July 2011, showing the 25 m high proximal scar of the 100 m diameter crater; (G) Crater 25 (Muldalen) in August 2011, a small crater (25 m diameter) with a 4 m high distal mound (covered with small trees of mountain birch, left background); (H) a very small (diameter 5 m) 'secondary crater' with a boulder pile at its distal edge (note the distal mound of Crater 25 in the background).

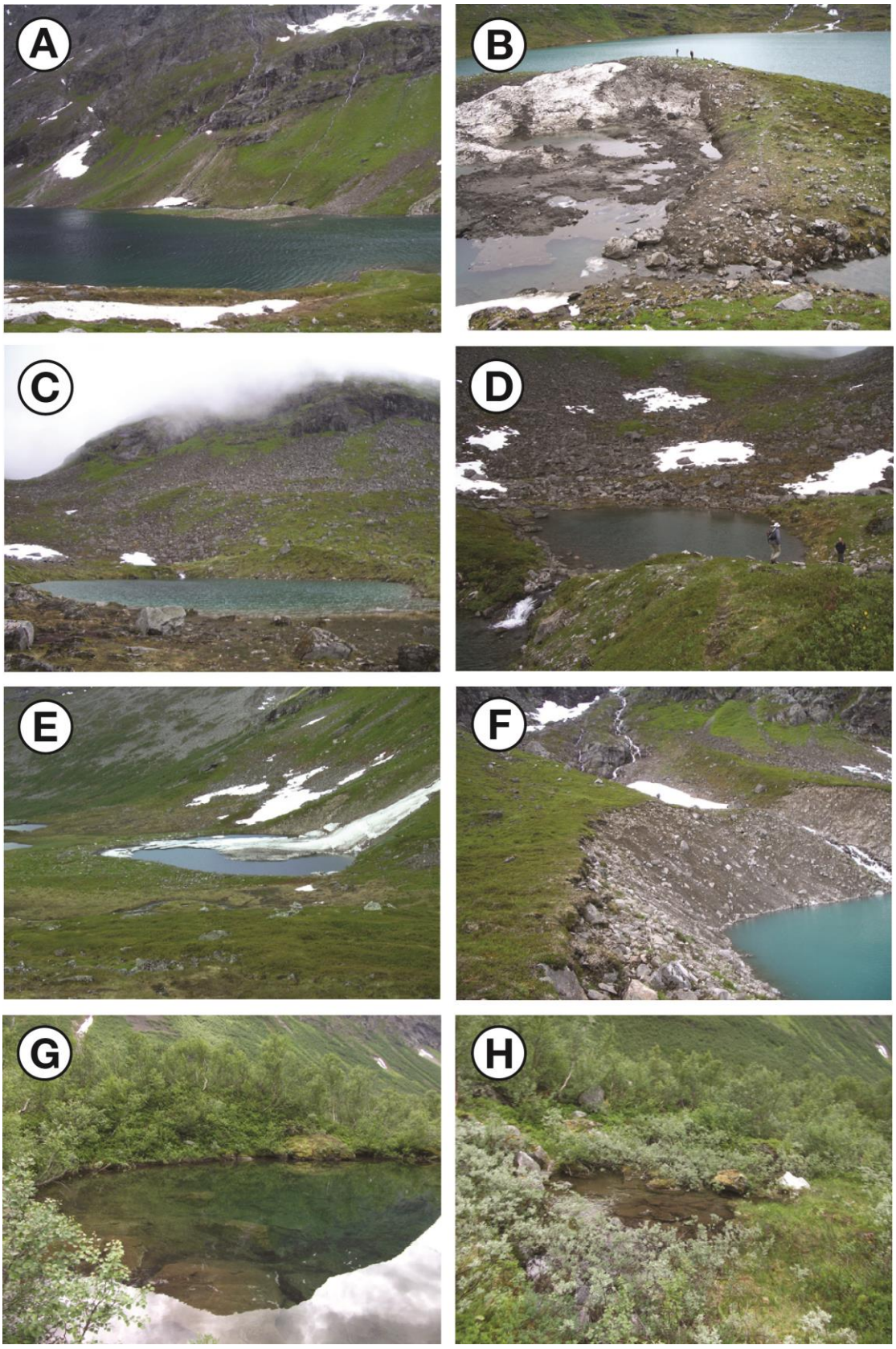

1406

1407

Fig. 6. Further terrestrial photographs of selected craters: (A) Crater 28 (Norangsdalen) in July 1999, showing the proximal scar (height 15 m) eroded in a colluvial fan; (B and C) Crater 31 (Norangsdalen) in July 1999,with a semi-circular, vegetated proximal scar (height 20 m) and pool, a low, multiple-crested distal mound, and surviving avalanche snow; (D) Crater 33 (Norangsdalen) in July 1999, a large, deep crater with a very extensive proximal scar (height 40 m) and relatively low distal mound and boulder spread in the foreground; (E) Crater 50 (Nøkkvatnet) in July 2011 showing part of the elongate pool and birch tree-covered distal mound; (F) Crater 51 (Skjærdingsdalen) in August 2011, showing the distal mound and the plunge pool partly infilled by the toe of a colluvial fan (right).

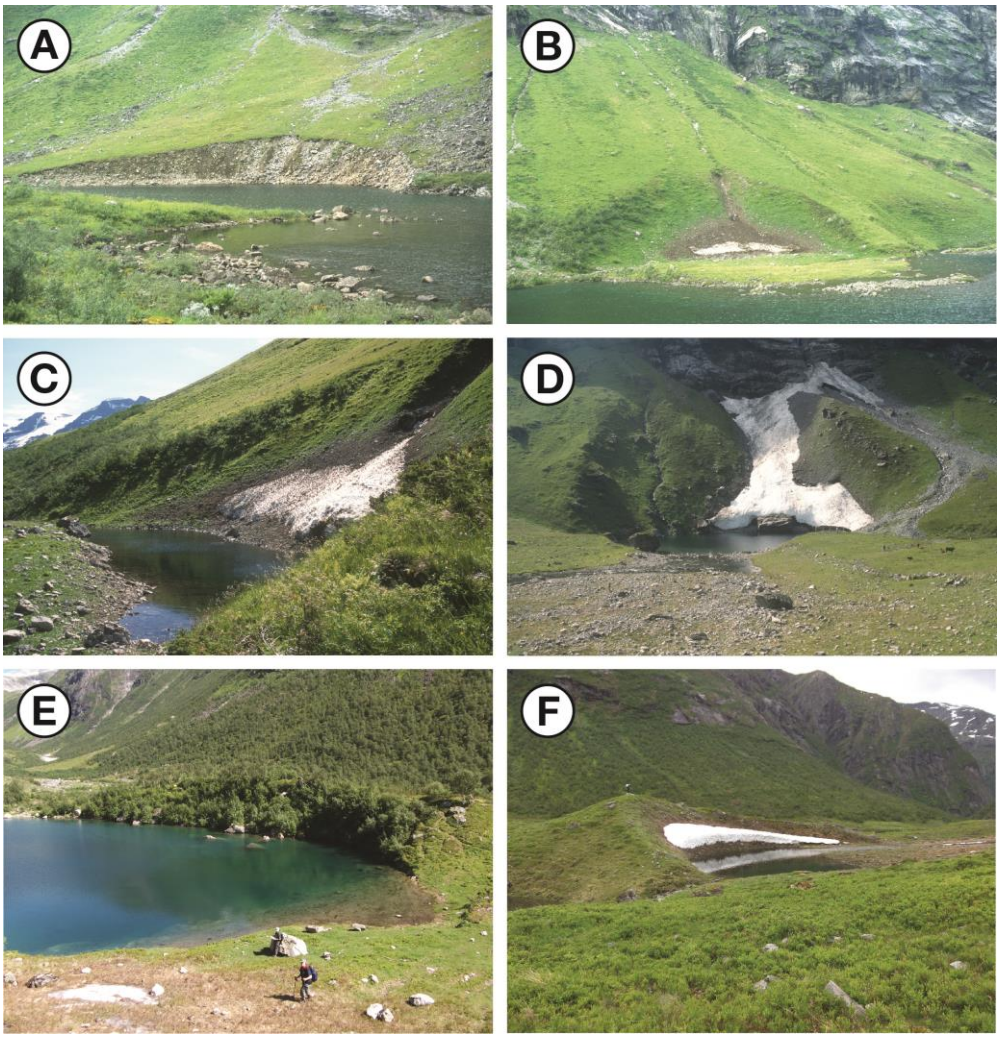

Fig. 7. Profiles of the avalanche paths (start point to crater) associated with 52 snow-avalanche craters.

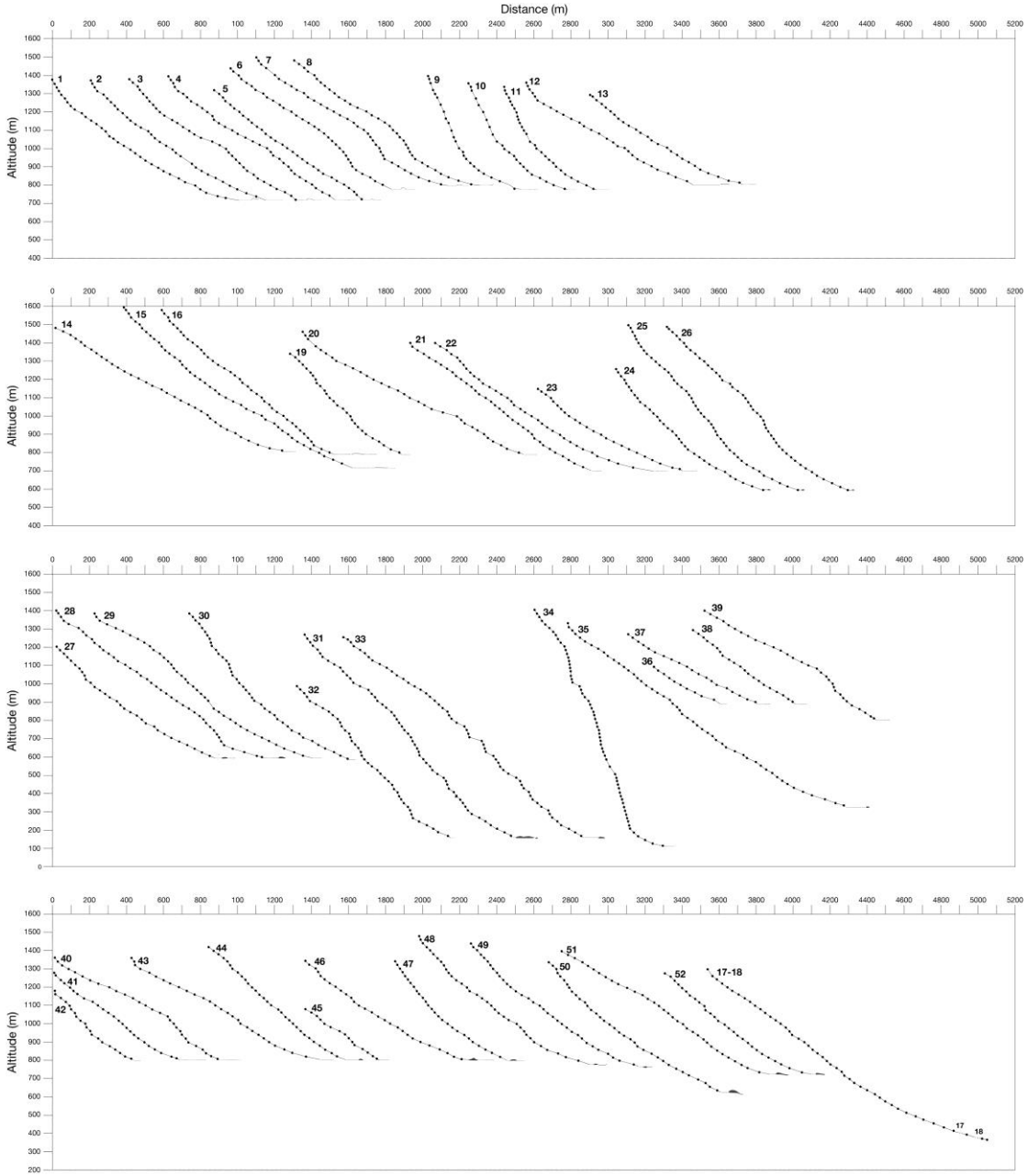

Fig. 8. Frequency histograms and rose diagram summarizing morphological and topographic parameters for 52 snow-avalanche craters and associated topography: (A) crater diameter; (B) crater wall height; (C) start zone area; (D) vertical drop of the avalanche path; (E) path angle; (F) lower path angle; (G) path length; (H) path aspect.

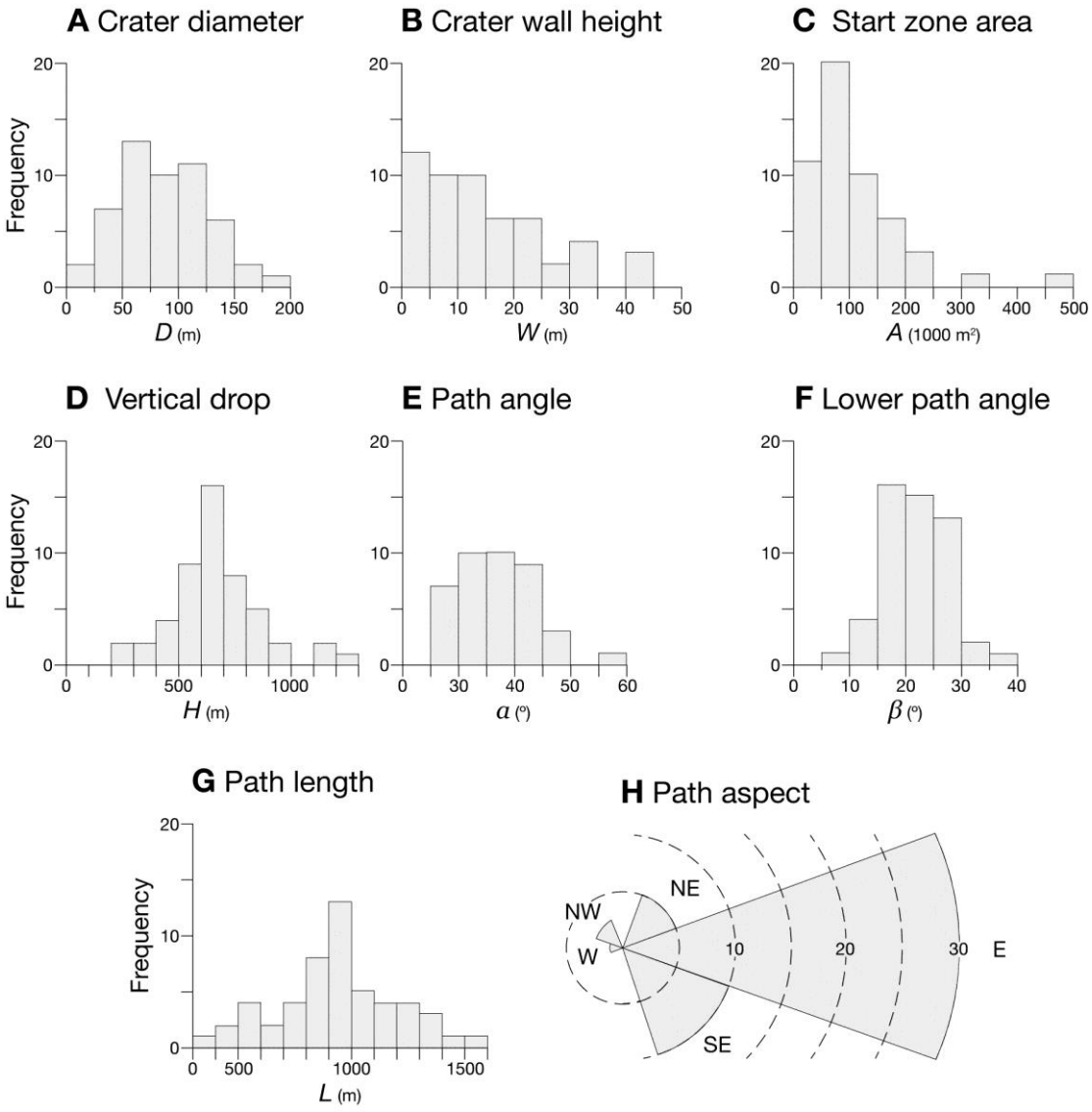

Table 1 Morphological and topographic parameters for the 52 snow-avalanche craters. Symbols are defined in the text. Crater wall height (W) refers to proximal scar height (w_p) except where distal scar height (w_d) is higher, as indicated.

Crater No.	D (m)	W (m)	A (1000 m^2)	Aspect (8-point)	H (m)	L (m)	α (°)	β (°)
1	75	4(w_d)	107	E	660	1040	33	11
2	110	1	69	E	660	1000	33	17
3	100	20	99	E	660	935	35	26
4	140	30	105	E	680	945	36	29
5	65	10	26	W	600	835	36	32
6	110	30	94	SE	665	900	36	25
7	80	8(w_d)	71	SE	705	1060	34	17
8	35	2(w_d)	43	SE	685	965	33	14
9	110	15	69	NW	625	555	47	17
10	60	7	23	NW	585	565	46	22
11	80	12	26	NW	565	550	46	23
12	140	20	179	SE	560	970	30	16
13	100	10	89	W	490	855	30	16
14	80	10	245	W	680	1260	28	15
15	160	20	97	S	885	1300	34	17
16	170	30	105	SE	790	970	38	27
17	10	2	115	E	890	1370	33	19
18	15	2	115	E	915	1460	32	18
19	70	12	89	E	550	630	41	26
20	100	25	324	NE	670	1220	28	19
21	60	8	102	E	700	1005	34	24
22	70	4	217	E	700	1210	29	9
23	95	12	94	NE	450	815	28	16
24	30	3(w_d)	130	SE	660	805	38	23
25	25	4(w_d)	89	SE	900	920	43	23
26	30	5(w_d)	82	SE	880	985	41	25
27	40	5	68	E	615	875	34	22
28	115	15	168	E	815	1160	34	14
29	60	3	117	E	795	1200	33	18
30	50	4	25	E	800	810	42	24
31	110	20	97	E	1110	1125	43	26
32	55	15	33	E	760	830	44	27
33	140	40	202	E	1100	1305	43	37
34	55	4	43	NE	1295	715	59	23
35	140	20	467	E	1010	1550	32	15
36	60	5	18	E	210	375	28	23
37	100	15	59	E	390	730	28	23
38	85	15	38	E	410	580	33	28
39	95	15	79	NE	600	955	32	28
40	140	30	77	NE	560	940	30	23
41	185	40	110	E	480	760	32	16
42	70	10	41	E	380	440	41	29
43	110	8	161	E	560	1050	28	13
44	140	20	173	E	620	770	38	24

45	75	10	48	E	280	420	32	32
46	60	8(w_d)	140	E	540	885	31	20
47	75	10	153	SE	540	620	41	28
48	30	4	89	E	700	930	36	18
49	60	5	77	E	670	925	35	21
50	115	40	94	SE	710	935	36	27
51	70	12(w_d)	184	E	670	1125	30	20
52	45	8(w_d)	61	E	550	1125	34	19
Mean	84.6	13.2	108.2	-	672.7	928.0	35.6	21.6
Median	77.5	10.0	94.0	-	662.5	935.0	34.0	22.5
Max.	185	40	467	-	1295	1550	59.0	37.0
Min.	10	1	18	-	210	375	28.0	9.0
SD	40.7	10.3	79.14	-	201.2	260.5	6.2	5.8
Skew	0.39	1.18	2.34	-	0.60	0.03	1.30	0.18

Table 2 Correlation coefficients (Pearson's r and Spearman's rho) between measures of crater size and characteristics of avalanche paths. Statistically significant coefficients are shown in bold: *** p<0.02; ** p<0.05; * p<0.10. Symbols are defined in the text.

	A	*H*	*L*	*α*	***β***
Pearson					
D	**0.312****	-0.038	0.073	-0.151	0.028
W	**0.249***	0.048	0.048	-0.024	**0.342*****
Spearman					
D	**0.338*****	-0.109	0.113	-0.154	-0.006
W	**0.227***	-0.179	-0.017	0.028	**0.338*****

Table 3 Summary of the modelling of the kinetic energy of snow-avalanche and meteorite impacts associated with a crater of 85 m diameter.

	Snow avalanche	**Small meteorite**
Mass (kg)	1.0×10^{7}	1.0×10^{4}
Velocity (m/s)	2.5×10^{1}	5.0×10^{3}
Kinetic energy (J)	3.1×10^{9}	1.3×10^{11}

1502 **Table 4** Confirmed small terrestrial meteorite craters.
1503

Site	No. of craters	Crater diameter (m)	**Sources**
Australia			
Henbury, NT	13	6–146	Hodge 1965; Buhl and McColl, 2015
Boxhole, NT	1	170	Milton 1968; Haines 2005
Dalgaranga, WA	1	20	Nininger & Huss 1960; Hodge 1994
Veevers, WA	1	70	Bevan and McNamara 1993; Hodge 1994
Hickman, WA	1	250	Glikson et al. 2008
North America			
Odessa, Texas	5	3–170	Hodge 1994; Holliday et al. 2005
Haviland, Kansas	1	17	Nininger and Figgins 1933; Hodge 1994
Whitecourt Alberta	1	36	Herd et al. 2008; Kofman et al. 2010
South America			
Campo del Cielo,	20	20–105	Hodge 1994; Cassidy and Renard 1996
Argentina	1	14	Kenkman et al. 2009; Tancredi et al. 2009
Carancas, Peru			
Africa and Middle East	3	11–116	Hodge 1994; Prescott et al. 2004
Wabar, Saudi Arabia	1	45	Folco et al. 2011; Buhl and McColl 2015
Kamil, Egypt			
Asia	122*	0.5–27	Krinov 1963; Hodge 1994
Sikhote-Alin, Russia	5	60-300	Gurov & Gurova 1998
Macha, Russia	1	50	Khryanina 1981; Hodge 1994
Sobolev, Russia	1	45	Petaev 1991; Buhl and McColl 2015
Sterlitanak, S. Bashkiria			
Europe	30	up to 120	Ormö et al. 2006
Sirente, Italy	9	12-110	Tiirmaa 1992; Raukas and Stankowski 2011
Kaali, Estonia	8	15-100	Classen 1978; Kuźmiński 1980
Morasko, Poland	3	24-80	Raukas et al. 2001; Plado 2012
Ilumetsa, Estonia			

1504 * Numerous additional ‘impact holes’ are <0.5 m; 24 of the 122 craters are 8.5–27 m.
1505